Frequency response based identification of nonlinear oscillators

Thomas Breunung[a,*], Balakumar Balachandran[a]

[a]*Department of Mechanical Engineering, University of Maryland, College Park, Glenn L. Martin Hall, 4298 Campus Drive, Maryland 20742, College Park, United States*

Abstract

Experimental modal analysis is commonly used to identify models for the vibratory behavior of structures. This is done by conducting a set of experiments to obtain the structure's governing equations and information in the form of eigenfrequencies, mode shapes, and damping. However, linearity of the test structure is assumed within this identification procedure. Hence, as it stands, experimental modal analysis is not readily applicable to build models when nonlinearities are present through, for example, friction, (electro-) magnetic fields, or large deformations. To identify governing equations for such systems, a robust and systematic identification procedure is proposed in this article. The identification routine is formulated in the frequency domain, and a noise reduction scheme and a simplification routine are employed to obtain sparse and robust models. The identification procedure is implemented in an automated script (FrID), which is applied to forced response measurements stemming from structures with magnets, clamps, and bolted joints as well as systems with multiple active modes and internal resonances. The identified governing equations accurately fit the experimentally obtained frequency response measurements and can also be utilized to extrapolate the response for different forcing amplitudes. Moreover, nonlinear modes of the underlying conservative system can be computed from the identified governing equations.

Keywords: system identification, frequency response curve, structural dynamics, multi-degree-of-freedom systems, nonlinear vibrations, experimental modal analysis

1. Introduction

The dynamic behavior of structures is commonly assessed via modal analysis and the associated experimental implementation, which is referred to as experimental modal analysis [1]. Assuming linearity of the test structure, the considered system is characterized via a set of mode shapes, eigenfrequencies, and possibly, damping ratios. However, in many engineering applications, phenomena such as backlash, fluid-structure interactions, or joint friction introduce discernible nonlinear behavior. The associated dynamics cannot be adequately captured with linear models stemming from experimental modal analysis. Unfortunately, no universal methodology to derive governing equations of nonlinear, oscillatory equations from experimental measurements is currently available.

During modal testing, structures are most commonly excited by exciters or impacts. Within impact testing, the structure is excited by a hammer or impactor and the free, decaying structural response is recorded. Such tests can be conducted quickly and require limited instrumentation. Hence, free-decay measurements remain an appealing procedure for testing nonlinear structures. For example Nonlinear AutoRegressive Moving Average models with eXogenous inputs (i.e. NARMAX-models) [2], the Hilbert transformation [3], and methods based on extraction of zero-crossings [4] have been utilized to identify nonlinear oscillators from free-decay measurements. However, most of these methods have been developed for single degree-of-freedom systems. Notably, NARMAX models can be built for multi-degree-of-freedom systems. An application of

*Corresponding author

Email addresses: thomasbr@umd.edu (Thomas Breunung), balab@umd.edu (Balakumar Balachandran)

such black-box models to vibration data remains challenging, as these approaches can result in unstable models [5]. Moreover, the repeatability of impact testing is a fundamental issue [1]. Hence, the results need to be verified via laborious repetitions (e.g., [6]).

On the other hand, shaker testing is highly repeatable and controllable. Thus, this testing type is a natural candidate for the characterization of nonlinear systems, despite the considerable instrumentation needed and possible shaker-structure interactions [7]. A variety of excitations such as (pseudo-) random, periodic, or sine-sweep/chirp signals can be generated with shakers. Out of these excitation signals, periodic forcing has received considerable attention, and hence, the response of nonlinear systems to periodic forcing has been extensively studied (e.g., [8–10]). Moreover, forced response curves, defined as the structure's steady state response to harmonic excitation, are a vital part of, for example, turbomachinery design [11, 12], automotive testing [13], and performance evaluations of (aero-) space structures [14, 15]. Therefore, it is of utmost importance to derive nonlinear models that accurately fit forced response measurements.

Feldman [16] proposed a method to identify amplitude dependent damping and eigenfrequencies of a single-degree-of-freedom system based on forced response measurements. Therein, the Hilbert transformation is employed. This signal transformation can be, most appropriately, interpreted as shifting the signal's phase by $\pi/2$. While this method has been used for identification of nonlinear systems [17], it is fundamentally limited to responses with a single active mode. To a certain extent, this limitation can be overcome by filtering a multi-mode response. However, the effects of modal interactions (e.g., [18, 19]), internal resonances, and closely spaced modes cannot be captured.

Higher order transfer functions offer another approach to nonlinear system identification (e.g., [20–22]). The theoretical underpinning of such approaches is the representation of input-output relationships of nonlinear systems in Volterra series [23]. Volterra series can be interpreted as a nonlinear extension of the Dunhamel integral. By transforming the Volterra series to the frequency domain, one obtains higher order transfer functions. These functions can be experimentally determined by using either harmonic or random inputs [24]. However, the convergence properties of the generally infinite Volterra series are unclear. Furthermore, frequency responses of nonlinear systems with multiple coexisting responses cannot be captured with Volterra series.

Polynomial nonlinear state-space models have been utilized to model dynamics in the discrete time domain [25]. Therein, the dynamics are approximated by polynomials of the past states and past control inputs. As such, those models represent a subclass of NARMAX models and they have been extensively used to model, for example, hysteretic systems [26], aero-engine components [27], flow-induced vibrations [28], and wing systems [29]. However, based on Volterra series one assumes a unique steady state response in this modelling approach [25]. Thus, systems with multiple, coexisting steady states, often observed in nonlinear structural dynamics [8, 30, 31] cannot be captured. Moreover, it has been observed that the obtained models are strongly input-dependent and perform poorly for forcing close to nonlinear resonances [5, 32].

Alternative system identification methods rely on the concept of so called nonlinear normal modes [30, 33]. These nonlinear modes are families of periodic orbits of conservative systems and their frequency-amplitude relationship has been denoted as a nonlinear continuation of eigenfrequencies. Methods such as response-controlled stepped-sine testing [34], control-based continuation [35], and phase-locked-loop testing [36] have been used to experimentally identify nonlinear modes and examine the dynamics of nonlinear oscillators. With the help of control algorithms, a detailed picture of the forced response curve, including even unstable branches, can be obtained. Recently, nonlinear modes have been utilized to perform model selection and updating in a Bayesian framework [37]. However, the reliance on a control strategy adds additional experimental complexity. Furthermore, these methods are restricted to response patterns that can be approximated by a single vibration mode.

Furthermore, system identification methods relying on restoring surfaces have been proposed [38]. Initially Chebyshev series expansion have been utilized to approximate nonlinearities. Subsequently, this expansion has been replaced with polynomials of the states [39] and extensions to multi-degree-of-freedom systems have been proposed [40]. Recently, the restoring surface method has been coupled with reduced order modelling strategies [41] and subspace identification methods [42]. These methods allow for visualization of the nonlinearities, which in turn can yield valuable insights. However, the restoring surface method has

high demands on the quality of the supplied data [43] and often requires additional steps to find numerically stable solutions [44].

Similarly, Adams and Allemang [45] propose a nonlinear system identification technique by interpreting the nonlinearity as an internal feedback loop. This frequency domain technique was subsequently converted to the time domain [46] to leverage the robustness and performance of subspace algorithms. Later, Kerschen and Noël [47] proposed a frequency domain subspace identification routine. These techniques have been applied, for example, to space structures [48]. Moreover, the identified models can be utilized to compute forced response curves based on the harmonic balance procedure coupled with continuation techniques [49]. Recently, the feedback interpretation has also been combined with a Kalman filter identification procedure [50]. However, with all of these methods, one assumes that the functional form of the nonlinearities is exactly known.

Yasuda and collaborators [51–53] have utilized the harmonic balance procedure to identify systems from simulated data. Subsequently, Feeny *et al.* [54] have applied Yasuda's method to identify a model for a forced magneto-elastic resonator operating in the chaotic regime. However, the obtained eigenfrequencies and damping values differ significantly from the corresponding actual values. In other applications [55–58], researchers have resorted to specific, single degree-of-freedom models. Recently, similar techniques have been applied to isolated resonances of multi degree-of-freedom systems [44] yielding a set of candidate models. Therein, the functional form of the equation of motion is generally assumed to be known and only the parameter estimation is performed. However, the detection and characterization of the nonlinearity, which are other essential steps of the system identification process [17], have not been carried out.

The general equation discovery tool SINDy [59] could be utilized to obtain governing equations from measurements. However, SINDy is sensitive to noise, and hence, primarily applied to synthetic data sets [59, 60]. Therefore, additional modifications of the originally formulated sparse regression have been proposed, and applications to some experimental data have been reported [61–68]. However, in all the applications reported, the underlying regression is formulated in the time domain. For modal testing of linear systems, on the other hand, time-domain and frequency-domain based methods have been proven to be successful in practice [1, 7, 69]. Therein, each domain is associated with unique advantages. Thus, it is expected that both domains will be of importance when testing nonlinear structures. However, sparse regressions algorithms have been exclusively formulated in the time domain.

To overcome some of these limitations, a robust system identification procedure to deduce governing equations of nonlinear oscillators from the frequency responses data is presented and experimentally validated in this article. Therein, the advantages of frequency domain for structural dynamics are combined with model selection algorithms formulated for general dynamical systems in the time domain. As such, the proposed method can be viewed as a frequency-domain extension of the popular SINDy algorithm [59] for structural dynamics. More specifically, the identification procedure is performed in the frequency domain and linear as well as nonlinear terms are modeled via a rich base of library functions (cf. Section 2.3). This modelling approach results in a set of linear equations, and a least squares solution is sought. To this end, noise reduction and simplification routine are employed to obtain interpretable and robust governing equations, which accurately capture the measured forced response (cf. Section 2.4). Thereby, all three steps of nonlinear system identification, which are detection, characterization, and parameter estimation [17], are performed. This procedure is implemented in an automated script FrID[1] (cf. Section 2.5).

The capabilities of the identification routine are illustrated through application to different nonlinear oscillators (cf. Section 3). Within these experiments, magnets (Section 3.1), clamps (Section 3.2), and bolted joints (Section 3.3) cause nonlinear behavior. The identified nonlinear oscillatory equations are interpretable, and the emergence of the identified terms can be related to physical sources. The derived governing equations prove to be robust, and the responses can be extrapolated for different forcing levels. Moreover, conservative nonlinear modes can be computed from the identified models. In addition to single degree-of-freedom systems, FrID is applied to experiments with two and three closely spaced modes (cf. Section 3.1.2), and notably, a structure with an internal resonance (cf. Section 3.1.3). Also, for these systems, the obtained governing

[1]The MATLAB script FrID is publicly available at `https://github.com/tbreunung/FrID`.

equations accurately capture the individual modes as well as their interactions. Overall, nonlinear oscillators from frequency response measurements are reliably identified, and thus, a pathway to experimental nonlinear modal analysis is provided.

2. Methods

Due to the importance of the forced response in applications, it is natural to employ such measurements to identify the governing equations of nonlinear structures. This motivates the system identification procedure proposed in this article. More specifically, an algorithm is developed to obtain sparse governing equations from a set of forced response measurements of a nonlinear structure.

In the following, the utilized class of models (cf. Section 2.1) and the required forced response measurements are described (cf. Section 2.2). Both are subsequently transformed into the frequency domain (cf. Section 2.3) yielding a set of linear equations for system identification (cf. Section 2.4). Within the proposed identification procedure, the effects of noise are reduced (cf. Section 2.4.1), linear dependencies are removed (cf. Section 2.4.2), and a simplification routine is carried out (cf. Section 2.4.3) to yield sparse and robust governing equations of nonlinear structures. These steps then are collected into an automated algorithm, which is described in Section 2.5.

2.1. Nonlinear oscillator models

In the following, the general class of nonlinear oscillatory systems

$$\ddot{\mathbf{q}} + \mathbf{N}(\dot{\mathbf{q}}, \mathbf{q}) = \mathbf{f}(t; \Omega), \qquad \mathbf{q} \in \mathbb{R}^N, \tag{1}$$

is fitted to measured forced response curves. The vector $\mathbf{q}$ consists of the generalized coordinates and $\mathbf{f}(t;\Omega)$ is the vector associated with the external forcing. The internal forces $\mathbf{N}(\dot{\mathbf{q}}, \mathbf{q})$ in equation (1) depend on the position $\mathbf{q}$ and velocity $\dot{\mathbf{q}}$ and can include linear and nonlinear stiffness, damping, and potentially, additional terms. The internal forces are modeled as the sum

$$\mathbf{N}(\dot{\mathbf{q}}, \mathbf{q}) := \sum_{p=1}^{P} \mathbf{N}^p g_p(\dot{\mathbf{q}}, \mathbf{q}), \tag{2}$$

where the parameter vectors $\mathbf{N}^p$ are unknown and $g_p(\dot{\mathbf{q}}, \mathbf{q})$ denote known, scalar functions, which are referred to as library functions. The choice of the library function can be based on, for example, physical insights or experimental experience. In general, the functions $g_p(\dot{\mathbf{q}}, \mathbf{q})$ can contain linear and nonlinear terms and can include conservative terms as well as non-conservative terms (i.e., damping). A natural candidate for the library functions are polynomials, which can approximate any continuous, real-valued function (cf. Stone-Weierstrass Theorem in, e.g., [70]). Hence, polynomial functions have been extensively used in the modeling of nonlinear oscillators (cf., e.g., [8]). It is generally recommended to include a variety of library functions so that the measured response can be easily captured. In the upcoming developments, it is shown how possible redundancies, spurious parameters, and overfitting are automatically avoided.

Model (1) is formulated in a set of coordinates so that the mass matrix is the identity matrix. This is not a restriction, since mechanical systems with non-identity mass matrix $\mathbf{M}$ can be converted into the model (1) by, for example, right multiplying the equations of motion with $\mathbf{M}^{-1}$. Thus, instead of assuming a model with non-identity mass matrix $\mathbf{M}$, one can assume model (1) without loss of generality. An important consequence of this observation is that the linear part of $\mathbf{N}$ that is proportional to the displacement $\mathbf{q}$ is generally not a positive definite stiffness matrix $\mathbf{K}$, rather, the general matrix $\mathbf{M}^{-1}\mathbf{K}$.

2.2. Shaker testing

To obtain forced response curves of structures via shaker testing, a periodic signal is supplied to the exciter and the resulting periodic steady state vibrations are measured. In the following, the forcing period is denoted by T and the angular frequency by $\Omega = 2\pi/T$. For each frequency, measurements from N different

structural locations can be taken (e.g., with multiple or roving sensors). These multi-channel signals are grouped into the signal vector

$$\mathbf{s}_m(t;\Omega_m) = \begin{cases} \mathbf{q}_m(t;\Omega_m) & \text{position measurement} \\ \dot{\mathbf{q}}_m(t;\Omega_m) & \text{velocity measurement} \\ \ddot{\mathbf{q}}_m(t;\Omega_m) & \text{acceleration measurement} \end{cases}, \qquad m = 1, ..., M, \tag{3}$$

which is indexed with the integer m since such steady state measurements are repeated for various excitation frequencies Ω_m. The total number of measurements is denoted by M. For vibration testing, these signals $\mathbf{s}_m$ are generally positions $\mathbf{q}_m$, velocities $\dot{\mathbf{q}}_m$, or accelerations $\ddot{\mathbf{q}}_m$ as indicated in equation (3).

It is assumed that for each generalized coordinate in equation (1), a corresponding measurement is taken (cf. equation (3)). Sometimes more measurements than the number of degrees of freedom (i.e., modes) are taken to resolve mode shapes [7]. In other applications, for example, structural health monitoring, the number of channels can be less than the number of degrees of freedom. Both of these scenarios; that is, more sensors than the number of degrees of freedom and less measurements than the number of degrees of freedom, can be considered in the future.

In the following, it is assumed that only position, velocity, or acceleration measurements are available. Notably, no measurement of the excitation is required. Only periodicity of the excitation needs to be ensured. This assumption is motivated by the most elementary shaker test set-up, wherein a periodic signal is supplied to the exciter, but the exact amplitudes of the resulting force acting on the test structure are unknown. Of course, load cells can be used to measure the force acting on the structure.

2.3. Frequency domain

Periodic signals are most appropriately described in the frequency domain. In practice, a time series of a periodic signal consisting of thousands of samples can be accurately represented with a few amplitudes. This explains the popularity of the frequency domain in vibration engineering. Furthermore, sophisticated signal processing and filtering tools are available for enhancing the signal to noise ratio. In this spirit, the external excitation is expanded in a Fourier series

$$\mathbf{f}(t;\Omega) = \sum_{k=-K}^{K} \mathbf{f}^{(k)} e^{\mathrm{i}k\Omega t}, \tag{4}$$

wherein the complex amplitudes $\mathbf{f}^{(k)}$ are unknown since no measurement of the forcing is available. In shaker testing, often sinusoidal signals are supplied to the exciter, and hence, it is reasonable to assume that the generated forcing can be modeled with a single harmonic. However, it is well known that vibration exciters commonly excite higher harmonics [71]. To account for such effects, higher harmonics are included in the Fourier series expansion (4) of the external periodic forcing.

The exponential functions in the Fourier series in equation (4) are selected for notational convenience. The expansion (4) as well as the upcoming developments can be equivalently formulated by utilizing trigonometric functions (i.e., sine and cosine functions).

In the frequency domain, velocity and acceleration signals can be recovered from measurements of the position. The Fourier transformation

$$\mathbf{q}_m^{(k)} := \frac{1}{T} \int_0^T \mathbf{q}_m(t;\Omega_m) e^{-\mathrm{i}k\Omega_m t} \, dt, \tag{5}$$

yields the complex amplitudes $\mathbf{q}_m^{(k)}$. The Fourier-integral (5) can be evaluated via the FFT-algorithm or by numerical quadrature of the integral (5)[2]. Both approximations introduce artifacts, most prominently

[2]In FrID, the integral (5) is approximated by using the right Riemann sum.

aliasing and spectral leakage [7, 10]. To avoid aliasing the sampling frequency needs to be chosen at least two times higher than the highest relevant frequency. In practice, higher sampling frequencies are preferred. Aliasing can be reduced by selecting appropriate filter functions [7, 10]. After utilizing equation (5), the velocities $\dot{\mathbf{q}}$ and accelerations $\ddot{\mathbf{q}}$ can be obtained as follows:

$$\begin{aligned} \mathbf{q}_m(t;\Omega_m) = \sum_{k=-K}^{K} \mathbf{q}_m^{(k)} e^{\mathrm{i}k\Omega_m t}, \quad \Leftrightarrow \quad \dot{\mathbf{q}}_m(t;\Omega_m) = \sum_{k=-K}^{K} \mathrm{i}k\Omega_m \mathbf{q}_m^{(k)} e^{\mathrm{i}k\Omega_m t}, \\ \Leftrightarrow \quad \ddot{\mathbf{q}}_m(t;\Omega_m) = -\sum_{k=-K}^{K} k^2\Omega_m^2 \mathbf{q}_m^{(k)} e^{\mathrm{i}k\Omega_m t}. \end{aligned} \tag{6}$$

For measurements of the velocities and accelerations, similar conversions can be made. As indicated in equation (6), in the frequency domain, positions, velocities, and accelerations are easily converted without relying on numerical differentiation or integration. To convert the model for the internal forces $\mathbf{N}$ into the Fourier domain, the library functions g_p are projected onto the Fourier modes

$$g_{p,m}^{(k)} := \frac{1}{T}\int_0^T g_p(\dot{\mathbf{q}}_m(t;\Omega_m), \mathbf{q}_m(t;\Omega_m)) e^{-\mathrm{i}k\Omega_m t}\, dt, \tag{7}$$

wherein the positions $\mathbf{q}$ and velocities $\dot{\mathbf{q}}$ are either retained directly from the measurements $\mathbf{s}_m$ or via the conversion (6) from the Fourier coefficients $\mathbf{q}_m^{(k)}$. After substituting the model (2) into equation (1) and utilizing the Fourier expansions of the library functions (7) and forcing (4), the result is

$$\sum_{k=-K}^{K} \left(-k^2\Omega_m^2 \mathbf{q}_m^{(k)} + \sum_{p=1}^{P} \mathbf{N}^p g_{pm}^{(k)} - \mathbf{f}^{(k)} \right) e^{\mathrm{i}k\Omega_m t} = 0, \qquad m = 1, ..., M, \tag{8}$$

whereby the parameter vectors $\mathbf{N}^p$ and forcing amplitudes $\mathbf{f}^{(k)}$ are unknown. It is noted that equation (8) is linear in these unknown parameters. Now, any periodic function $f(t)$ is equal to zero if and only if all its Fourier coefficients $f^{(k)}$ are identically zero. This fact can be deduced by observing that the Fourier transformation is invertible and that all Fourier coefficients of the Fourier transformation of zero are equal to zero. Applying these arguments to equation (8) implies that each summand of the left-hand side needs to be equal to zero yielding

$$-k^2\Omega_m^2 \mathbf{q}_m^{(k)} + \sum_{p=1}^{P} \mathbf{N}^p g_{pm}^{(k)} - \mathbf{f}^{(k)} \stackrel{!}{=} 0, \qquad -K \le k \le K, \qquad m = 1, ..., M. \tag{9}$$

Equation (9) can also be derived by a Galerkin projection of equation (8) onto its Fourier modes or by imposing harmonic balance [8, 72]. For the following developments, it is most illustrative to write down the j-th row of equation (9) for all Fourier modes between $-K$ and K which are given by

$$\begin{array}{cccccccc} -K^2\Omega_m^2 q_{jm}^{(-K)} & +N_j^1 g_{1m}^{(-K)} & +N_j^2 g_{2m}^{(-K)} & +... & +N_j^P g_{Pm}^{(-K)} & -f_j^{(-K)} & = 0, & \\ -(-K+1)^2\Omega_m^2 q_{jm}^{(-K+1)} & +N_j^1 g_{1m}^{(-K+1)} & +N_j^2 g_{2m}^{(-K+1)} & +... & +N_j^P g_{Pm}^{(-K+1)} & -f_j^{(-K+1)} & = 0, & \\ \vdots & \vdots & \vdots & & \vdots & \vdots & \vdots & m = 1, ..., M. \\ -K^2\Omega_m^2 q_{jm}^{(K)} & +N_j^1 g_{1m}^{(K)} & +N_j^2 g_{2m}^{(K)} & +... & +N_j^P g_{Pm}^{(K)} & -f_j^{(K)} & = 0, & \end{array} \tag{10}$$

The unknowns in equations (10), which are the coefficients of the library functions N_j^1, N_j^2,..., N_j^P and the external forcing $f_j^{(-K)}$, $f_j^{(-K+1)}$,..., $f_j^{(K)}$, can be summarized in the following vector

$$\mathbf{p}_j := \left[N_j^1, N_j^2, ..., N_j^P, f_j^{-K}, f_j^{-K+1}, ..., f_j^K \right]^\top \in \mathbb{R}^{P+(2K+1)}. \tag{11}$$

Moreover, after introducing the notation

$$\mathbf{A}^m := \begin{bmatrix} g_{1m}^{(-K)} & g_{2m}^{(-K)} & ... & g_{Pm}^{(-K)} & -1 & 0 & ... & 0 \\ g_{1m}^{(-K+1)} & g_{2m}^{(-K+1)} & ... & g_{Pm}^{(-K+1)} & 0 & -1 & ... & 0 \\ \vdots & \vdots & \ddots & \vdots & \vdots & \ddots & \vdots & \\ g_{1m}^{(K)} & g_{2m}^{(K)} & ... & g_{Pm}^{(K)} & 0 & 0 & ... & -1 \end{bmatrix} \in \mathbb{R}^{(2K+1)\times P+(2K+1)},$$
$$\mathbf{B}_j^m := \left[K^2\Omega_m^2 q_{jm}^{(-K)}, (-K+1)^2\Omega_m^2 q_{jm}^{(-K+1)}, ..., K^2\Omega_m^2 q_{jm}^{(K)}\right]^\top \in \mathbb{R}^{2K+1}, \tag{12}$$

equations (10) can be summarized as

$$\mathbf{A}^m \mathbf{p}_j = \mathbf{B}_j^m, \qquad m = 1, ..., M. \tag{13}$$

Stacking the matrices $\mathbf{A}^m$ and vectors $\mathbf{B}_j^m$ for all M measurements as follows

$$\mathbf{A} := \begin{bmatrix} \mathbf{A}^1 \\ \mathbf{A}^2 \\ \vdots \\ \mathbf{A}^M \end{bmatrix} \in \mathbb{R}^{M(2K+1)\times P+(2K+1)}, \qquad \mathbf{B}_j = \begin{bmatrix} \mathbf{B}_j^1 \\ \mathbf{B}_j^2 \\ \vdots \\ \mathbf{B}_j^M \end{bmatrix} \in \mathbb{R}^{(2K+1)M}, \tag{14}$$

allows one to condense the equations (10) to

$$\mathbf{A}\mathbf{p}_j = \mathbf{B}_j, \qquad j = 1, ..., N, \tag{15}$$

for each coordinate j. The linear systems (15) are the fundamental equations for the proposed system identification procedure. If measurements of the excitation were available, they can be incorporated by deleting the last $2K+1$ columns of the matrices $\mathbf{A}^m$ (cf. equation (12)) respectively $\mathbf{A}$, deleting the last $2K+1$ entries of the vector with unknowns $\mathbf{p}_j$ (cf. equation (11)) and including the measured forcing amplitudes into $\mathbf{B}_j^m$ (cf. equation (12)) respectively $\mathbf{B}_j$. However, throughout this article, the amplitudes of the external forces are assumed to be unknown.

If enough measurements have been collected (at least $M > 1 + P/(2K+1)$), then the linear systems (15) are overdetermined and can be solved for the parameter vector $\mathbf{p}_j$ by minimizing the least squares errors, or equivalently, the geometric distance between $\mathbf{A}\mathbf{p}_j$ and $\mathbf{B}_j$. A similar procedure has been applied to less general equations than equation (1) in, for example, the studies [51–57]. However, this straightforward approach with the general model (2) will result in an overfit consisting of many spurious parameters, lacking extrapolation capabilities, limited interpretability and often yielding unstable simulation results. To overcome these shortcomings, a systematic treatment of noise as well as judicious simplification are employed.

2.4. Identification

The linear equations (15) serve as a starting point to identify nonlinear oscillatory equations of the form (1). Due to the introduction of an abundance of library functions (2) and measurement noise, three essential steps have to be carried out to yield a reliable identification procedure. In the first step, coefficients below the noise floor are truncated as described in Section 2.4.1. Subsequently, linear dependencies in the equations (15) are removed (cf. Section 2.4.2), and as a final step, spurious parameters are removed via a simplification routine in Section 2.4.3.

2.4.1. Noise

Any measurement is invariably corrupted by noise. To illustrate the employed, simple noise reduction procedure, a Fourier transformation of a prototypical measurement of a steady state response is shown in Fig. 1[3]. The excitation frequency is 39.5 Hz and the first three harmonics at about 40 Hz, 80 Hz, and 120

[3]The measurement shown in Fig. 1 stems from the experiment described in Section 3.1 and shown in Fig. 4.

Hz are clearly discernible. Higher harmonics from the fourth harmonic to the sixth harmonic (160 Hz, 200 Hz, and 240 Hz) can also be distinguished. The amplitudes of remaining higher harmonics (i.e., higher than six) and the amplitudes at frequencies that are at non-integer multiples of the excitation frequency of 39.5 Hz cannot be distinguished from the noise floor. This noise floor is estimated by calculating the amplitudes

$$\sigma(\Omega, m) := \frac{1}{TN}\left\| \int_0^T \mathbf{s}_m(t) e^{-\mathrm{i}k\Omega t}\, dt \right\|_1, \qquad \text{for } \Omega \quad \text{such that} \quad |n\Omega_m - \Omega| > 0.1\Omega_m, \tag{16}$$

where the last condition ensures that the frequency Ω is not an integer multiple of the excitation frequency Ω. The threshold value of $0.1\Omega_m$ ensures that Ω will be at least differ by 10% from the excitation frequency Ω_m and its integer multiples. This threshold value can be adjusted as appropriate. However, in their experiments, the authors have not observed any significant dependency of identified parameters on this threshold value. Equation (16) yields the average absolute value of the N amplitudes (i.e., one per each measurement channel). This is achieved by utilizing the 1-norm, which is a sum of the absolute values (rather than the squared absolute values as the standard 2-norm) and subsequently dividing by the number of entries N.

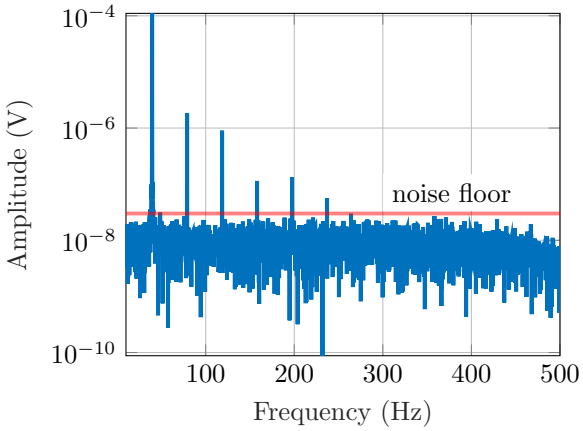

Figure 1: Representative amplitude spectrum of measured steady state response.

Generally, the value of the amplitude $\sigma(\Omega, m)$ will depend on the frequency Ω and the measurement m. An average noise floor is given by the expected value

$$\bar{\sigma} = \mathbb{E}(\sigma(\Omega, m)), \tag{17}$$

which is independent of the frequency Ω and the measurement m. The expected value (17) can be estimated by using the standard Monte-Carlo estimator; that is, by averaging over sufficiently many measurements m and frequencies Ω.

The constant noise floor shown in Fig. 1 can be related to the classical white noise model. For other noise models, for example, with frequency dependent intensities [73], the estimation technique (17) can be adjusted appropriately. The estimated noise floor (17) is utilized in two instances. First, when calculating the amplitudes $\mathbf{q}_m^{(k)}$ from the measurements $\mathbf{s}_m$ (cf. equation (5)), all entries with an absolute value less than two times the noise floor are set to zero, since these values cannot be reliably distinguished from the noise floor. This is done before reconstruction of the other measurements such as velocities or accelerations via equation (6) and before projecting the library functions on the Fourier modes in equation (7). Second, each entry of the matrix $\mathbf{A}$ and vectors $\mathbf{B}_j$ that is not at least two times larger than the noise floor is set to zero. This minimizes the number of spurious and unreliable coefficients in the linear equations (15). Hence, the identification procedure is robust to noise.

2.4.2. Linear dependencies

When equations (15) are solved for the least squares minimum, then, one essentially seeks a linear combination of the columns of the matrix $\mathbf{A}$ that approximates the vector $\mathbf{B}_j$ the best. This can be problematic, if two column vectors of $\mathbf{A}$ point in the same, or almost the same, direction, or more generally, the columns of $\mathbf{A}$ are linearly dependent. In this case, the identified parameters are not robust with respect to small changes in $\mathbf{A}$ and $\mathbf{B}_j$. To alleviate this problem, the column space of $\mathbf{A}$ is checked for linear dependencies iteratively.

Denoting the columns of $\mathbf{A}$ and entries of the parameter vector $\mathbf{p}_j$ as

$$\mathbf{A} = [\mathbf{a}_1, \mathbf{a}_2, ..., \mathbf{a}_{P+2K+1}], \qquad \mathbf{p}_j = \left[p_j^1, p_j^2, ..., p_j^{P+2K+1}\right]^\top, \tag{18}$$

then, a reduced matrix $\tilde{\mathbf{A}}$ without linear dependencies and reduced unknown vector $\tilde{\mathbf{p}}_j$ can be constructed iteratively as follows. Starting with the first column $\mathbf{a}_1$ the next column $\mathbf{a}_2$ is projected into the direction of $\mathbf{a}_1$. If the length of this projection is of similar length as the vector $\mathbf{a}_2$ then $\mathbf{a}_2$ primarily points in the direction of $\mathbf{a}_1$, and hence, both vectors are almost linearly dependent. If, on the other hand, the magnitude of the projection of $\mathbf{a}_2$ in the direction of $\mathbf{a}_1$ is small compared to the magnitude of $\mathbf{a}_2$, then the vectors $\mathbf{a}_1$ and $\mathbf{a}_2$ point in different directions. Only in this case the vector $\mathbf{a}_2$ and the corresponding unknown $\mathbf{p}_j^2$ are included in the reduced matrix $\tilde{\mathbf{A}}$ respectively vector $\tilde{\mathbf{p}}_j$.

For the remaining columns $\mathbf{a}_k$, this process is repeated. In this case, $\mathbf{a}_k$ is projected into the column space of $\tilde{\mathbf{A}}$. This projection is carried out by multiplying $\mathbf{a}_k$ with the projection matrix $\mathbf{P} = \tilde{\mathbf{A}}(\tilde{\mathbf{A}}^*\tilde{\mathbf{A}})^{-1}\tilde{\mathbf{A}}^*$. Here, the matrix $\tilde{\mathbf{A}}^*$ denotes the Hermitian transpose of $\tilde{\mathbf{A}}$ that is computed by transposing $\tilde{\mathbf{A}}$ and taking the complex conjugate of each entry. As illustrated in Fig. 2, the multiplication of $\mathbf{P}$ with $\mathbf{a}_k$ yields the vector $\mathbf{v}$, which is inside the column space of $\tilde{\mathbf{A}}$. Two distinct cases are shown in Fig. 2. For the column $\mathbf{a}_{k_1}$, the magnitude of the projection into the column space $\tilde{\mathbf{A}}$ is almost as large as the magnitude of $\mathbf{a}_{k_1}$, and hence, the column $\mathbf{a}_{k_1}$ is not included into $\tilde{\mathbf{A}}$ (cf. the vectors $\mathbf{a}_{k_1}$ and $\mathbf{P}\mathbf{a}_{k_1}$ in Fig. 2). The magnitude of the projection of $\mathbf{a}_{k_2}$ on the other hand is small compared to the length of $\mathbf{a}_{k_2}$, and hence, the column $\mathbf{a}_{k_2}$ will be included into $\tilde{\mathbf{A}}$ upon the next iteration.

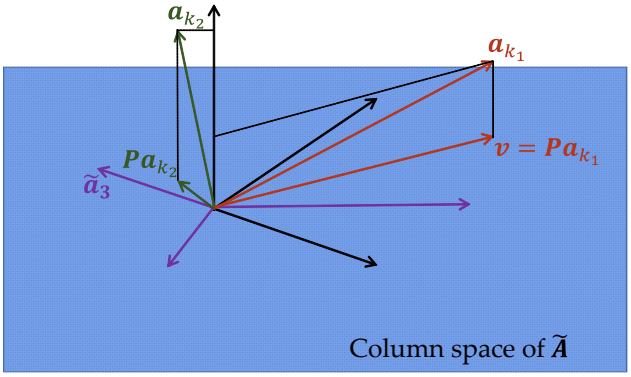

Figure 2: Linear projection into the column space of $\tilde{\mathbf{A}}$ utilizing the projection matrix $\mathbf{P}$. The column $\mathbf{a}_{k_1}$ has a large projection into the column space of $\tilde{\mathbf{A}}$, and hence, this column is not included in $\tilde{\mathbf{A}}$. The column $\mathbf{a}_{k_2}$ is almost orthogonal to the column space of $\tilde{\mathbf{A}}$ and hence will be included into $\tilde{\mathbf{A}}$.

An algorithmic implementation of the described procedure is given in algorithm 1, where the threshold to determine a different direction of the column $\mathbf{a}_k$ and its projection onto the column space of $\tilde{\mathbf{A}}$ is set to 0.95. The reduction algorithm 1 yields the following reduced linear system:

$$\tilde{\mathbf{A}}\tilde{\mathbf{p}}_j = \mathbf{B}_j. \tag{19}$$

Algorithm 1: Reduce linear dependencies

Result: Reduced matrix $\tilde{\mathbf{A}}$ and reduced parameter vector $\tilde{\mathbf{p}}_j$
$\tilde{\mathbf{A}} = \mathbf{a}^1$
$\tilde{\mathbf{p}}_j = p_j^1$
k=2
while $k \leq P + 2K + 1$ **do**
  $\tilde{\mathbf{A}}^* = \bar{\tilde{\mathbf{A}}}^\top$ // Compute the Hermitian transpose by transposing $\tilde{\mathbf{A}}$ and then complex conjugating each entry
  $\mathbf{P} := \tilde{\mathbf{A}}(\tilde{\mathbf{A}}^*\tilde{\mathbf{A}})^{-1}\tilde{\mathbf{A}}^*$ // Compute projection matrix
  $\mathbf{v} := \mathbf{P}\mathbf{a}_k$ // Project the k-th column of $\mathbf{A}$ into the column space of the reduced matrix $\tilde{\mathbf{A}}$
  if $|\mathbf{v}|/|\mathbf{a}_k| < 0.95$ **then** // Compare the length of $\mathbf{v}$ with magnitude of the column $\mathbf{a}_k$
    $\tilde{\mathbf{A}} = \left[\tilde{\mathbf{A}}, \mathbf{a}^k\right]$ // include $\mathbf{a}^k$ into the reduced matrix
    $\tilde{\mathbf{p}}_j = [\tilde{\mathbf{p}}_j, p_k]$ // update the parameter vector
  end
end

2.4.3. Simplification

After minimizing the effects of noise and reducing linear dependencies in the matrix $\mathbf{A}$, the vector of unknowns $\tilde{\mathbf{p}}_j$ in equation (19) still consists of numerous parameters due to the excessive use of library functions in the model of the internal forces (2). Hence, a least squares solution of equation (19) would result in complicated models with poor extrapolation capabilities and leading to, most likely, unstable simulation results. Thus, the number of unknowns in equation (19) needs to be reduced.

In the following, a simplification is in line with the sparsification for general dynamical system recently popularized in [59] and further advocated in [74]. Therein, it is argued that a sparsification yields not only simpler, but also more general models with better extrapolation capabilities. Various techniques for performing variable selection to obtain sparse models have been proposed. For example, Brunton *et al.* [59] propose to remove small coefficients. However, damping coefficients of mechanical oscillators are generally small, yet crucial to accurately capture the forced dynamics. Thus, the simplification strategy [59] appears to be inadequate for weakly damped, nonlinear oscillators. Alternatively, a ℓ_1 regularization of the least squares cost function has been advocated within the last absolute shrinkage and selection operator (LASSO) [75]. However, the arising optimization is difficult to solve, and numerical techniques have to be employed. Thereby, computation times become significant and additional tuning parameters arise.

A forward stepwise selection procedure [76, 77] is employed to reduce the unknowns $\tilde{\mathbf{p}}_j$ and obtain a sparse model (1). In the beginning of this procedure, a single entry of the vector $\tilde{\mathbf{p}}_j$ is selected to be non-zero. To determine the corresponding entry, a greedy algorithm is iterated through all entries of the vector $\tilde{\mathbf{p}}_j$ and the entry minimizing the least squares residual the most is selected. Then, the relative residual error

$$\frac{|\tilde{\mathbf{A}}_j\tilde{\mathbf{p}}_j - \mathbf{B}_j|}{|\mathbf{B}_j|}, \tag{20}$$

is compared to a predefined tolerance ε. If the relative residual error (20) is less than the error tolerance ε, then, the parameter selection is terminated. Otherwise, the procedure is continued and a second non-zero entry in the vector $\tilde{\mathbf{p}}_j$ is selected, while keeping the previously found entry constant. This procedure is repeated until the relative residual error (20) falls below the tolerance ε or all entries of the vector $\tilde{\mathbf{p}}_j$ are non-zero and the standard least squares fit is reached. The theoretical properties of forward stepwise algorithms are not well understood, but these algorithms generally perform very well in finding sparse subset of variables [77]. For asymptotically small error tolerances $\varepsilon \to 0$, the forward stepwise selection procedure leads to the standard least squares solution.

2.5. FrID: An automated identification package

The developments of the previous sections can be assembled into an automatic identification procedure yielding simple governing equations of nonlinear oscillators from frequency response measurements. A schematic overview is given in Fig. 3 and the following steps are implemented in the automated MATLAB script FrID[4]:

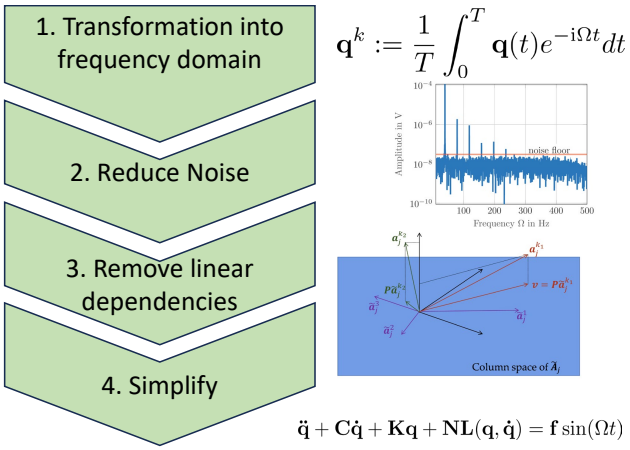

Figure 3: Overview of sequence of steps in system identification procedure implemented in FrID.

1. Frequency domain: Compute the Fourier series of the steady state responses and obtain the amplitudes $\mathbf{q}_m^{(k)}$ (cf. equation (5)).
   Remark: If amplitudes and phases are recorded, then the time signal can be deduced from those, or alternatively, the steps (2) and (3) can be omitted.
2. Reduce Noise: First, estimate the noise floor (cf. Section 2.4.1) and truncate the Fourier amplitudes $\mathbf{q}_m^{(k)}$ below the noise floor. Then, recompute the time series of the position and velocity of the steady state response and project the library functions $g_p(\dot{\mathbf{q}}, \mathbf{q})$ onto the Fourier modes (cf. equation (7)). For each degree of freedom, build the linear system (15) and set every entry of the matrix $\mathbf{A}$ and vectors $\mathbf{B}_j$ below the noise floor to zero.
3. Remove linear dependencies: Remove linear dependent columns of the matrices $\mathbf{A}$ (cf. Section 2.4.2).
4. Simplify: Identify a simple model by a forward stepwise selection, which successively leads to selection of non-zero coefficients in the parameter vector $\tilde{\mathbf{p}}_j$ that reduce the residual the most (cf. Section 2.4.3).

The library functions implemented in FrID are polynomials in the positions $\mathbf{q}$ and velocities $\dot{\mathbf{q}}$. For example, selecting a polynomial model of order two for a two degree-of-freedom system ($N = 2$) with the positions $\mathbf{q} = [q_1, q_2]^\top$ and velocities $\dot{\mathbf{q}} = [\dot{q}_1, \dot{q}_2]^\top$ yields a library consisting of the following 14 functions: q_1, q_2, $\dot{q}_1$,$\dot{q}_2$, q_1^2, q_1q_2, $q_1\dot{q}_1$, $q_1\dot{q}_2$, q_2^2, $q_2\dot{q}_1$, $q_2\dot{q}_2$, $\dot{q}_1^2$, $\dot{q}_1\dot{q}_2$, and $\dot{q}_2^2$. In general, for a N-degree-of-freedom system, by utilizing polynomials of order up to P one obtains the following number of library functions

$$\sum_{p=1}^{P} \binom{2N + p - 1}{p}. \tag{21}$$

Depending on the application, alternative library functions can be selected.

[4]FrID is publicly available at `https://github.com/tbreunung/FrID`.

3. Results and Discussion

The capabilities of the proposed identification procedure (implemented in FrID) are demonstrated by using response measurements from a variety of systems. First, magento-mechanical oscillator systems with one, two, and three degrees of freedom, including a configuration with an internal resonance are considered in Section 3.1. Subsequently, governing equations for the same mechanical oscillator without magnets are identified (cf. Section 3.2). As a final application example, FrID is applied to an external data set [78] of a beam with bolted joints (cf. Section 3.3).

Numerical simulations are utilized to validate the identified models. In general, the procedure of stepped sine testing (e.g., [7]) is emulated numerically. After selecting a starting frequency, the identified governing equations (1) are numerically integrated by using MATLAB's `ode45` routine and the integration is continued until a steady state is observed. This steady state is recorded, and then, the frequency is increased (stepped sine up) or decreased (stepped sine down) and the simulations are restarted from the previously observed steady state. This sequential continuation ensures that hysteric regions with multiple coexisting steady state responses can be explored. More advanced continuation packages, such as AUTO [79], COCO [80], or MATCONT [81] could be further utilized to reveal more detailed features of forced response curves, such as unstable branches. However, such solutions are generally not observable in experiments.

3.1. Magneto-mechanical Oscillator

As a first demonstration, FrID is applied to forced response measurements of the experiment shown in Fig. 4. The frame is moved horizontally via a shaker, and thereby, a base excitation is supplied to the mounted cantilevers. Magnets are attached to the end of each cantilever as well as on the opposite side at the frame. These magnets induce nonlinear force-tip-deflection relationships, which give rise to nonlinear forced response curves. The cantilever deflections are measured with strain gauges attached to the cantilevers close to the mount. Strain gauges are used to get a measure of the beam deformation. A strain gauge's output voltage is proportional to the local strain of the cantilever, which in turn can be related to the tip deflection of the beam. In the following, the strain gauge signal is treated as position measurement (cf. equation (3)), keeping in mind that the strain gauge signal is proportional to the tip deflection. The sampling frequency of the recorded strain gauge signals is 1.0 kHz.

In the experiments, a sinusoidal control signal is supplied to the shaker and the actual load acting on the structure is not measured. This set-up without a load cell resembles the most basic set-up of shaker testing. In some shaker tests, it is observed that the forcing level decreases close to resonance due to shaker-structure interaction. However, based on the specification of the utilized shaker (Brüel & Kjær 4811) and selected excitation mechanism (base excitation), it is reasonable to assume a constant forcing level for this experiment. Possible additional higher harmonics in the forcing are accounted for via the Fourier expansion of the external forcing (4).

A varying number of cantilevers can be mounted in the set-up shown in Fig. 4. Thereby, the capabilities of FrID for single and multi-degree-of-freedom systems can be evaluated. While the cantilevers are coupled through the base plate, the inter-cantilever coupling can also be enhanced by adding coupling springs as shown in Fig. 4. Macroscopically, all cantilevers have approximately the same properties, most importantly, eigenfrequencies of the excited first bending mode. As appropriate, magnetic masses can be attached to the cantilevers to shift these eigenfrequencies (cf., e.g., the far-right cantilever in Figure 4). This tuning allows one to observe closely spaced modes as well as structures with internal resonance.

In the following, several configurations of the experimental set-up shown in Fig. 4 are considered. First, a single cantilever is mounted and from the measured forced response a single-degree-of-freedom oscillator is identified with FrID. Subsequently, two and three cantilever systems are considered in Section 3.1.2 and multi-degree-of-freedom oscillators are identified with FrID. Finally, in Section 3.1.3, a structure with an internally resonance and two interacting modes is investigated.

3.1.1. Single degree-of-freedom system

After mounting a single cantilever in the experimental arrangement, supplying a periodic excitation, and varying the excitation frequency close to the cantilever's first bending mode frequency (approximately 40.0

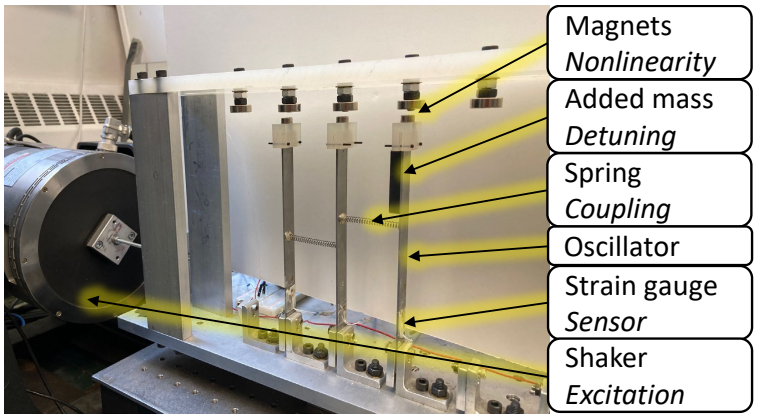

Figure 4: In-line oscillator experiment with three mounted cantilevers. The base plate is attached to an electrodynamic shaker.

Hz), the forced response shown in Fig. 5a is obtained. The excitation frequency is changed by 0.05 Hz every thirty seconds. This slow sweep rate is selected to ensure that the observed vibration patterns are close to a steady state. Depending on the sweep direction (increasing or decreasing the forcing frequency), different branches of steady state responses can be observed. Two distinct steady state responses are measured for excitation frequencies between 39.0 Hz and 41.0 Hz.

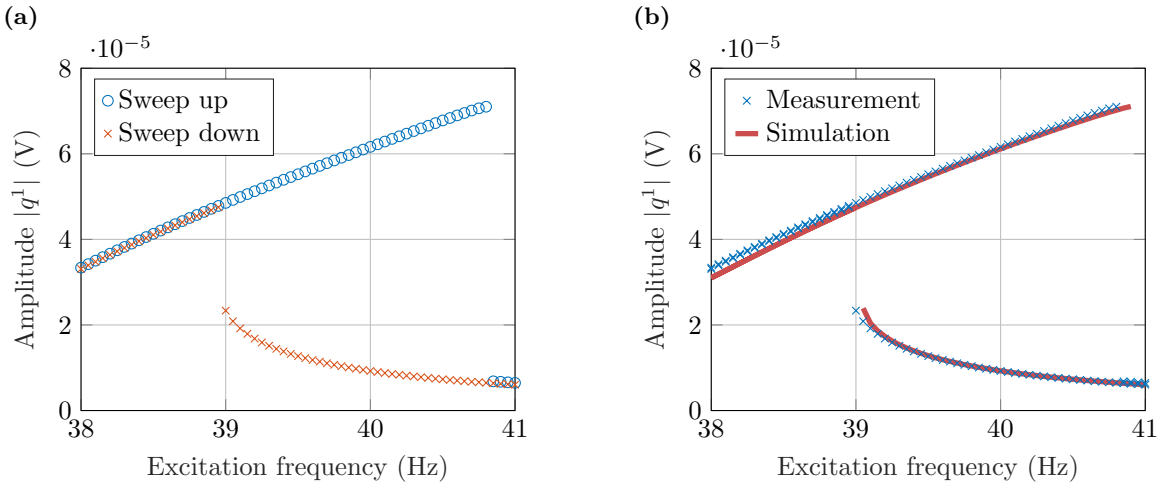

Figure 5: Single Cantilever System: (a) Measured forced response. (b) Measured and simulated forced responses.

On applying FrID to the measured forced response shown in Figure 5a, the result is the following model in non-dimensional coordinates

$$\begin{aligned} &\ddot{q} + c\dot{q} + kq + k_2 q^2 + k_3 q^3 = f\cos(\Omega t), \\ &c = 3.16, \qquad k = 56983.86, \qquad k_2 = 10141.92, \qquad k_3 = 15563.51, \qquad f = 733.96, \end{aligned} \tag{22}$$

where the non-dimensional coordinate q is related to the strain gauge voltage s by the factor $\alpha = 1.54{\cdot}10^{-4}$ V[5]

[5]The non-dimensionalization constant α is selected so that the maximal amplitude of the forced response in non-dimensional coordinates is equal to one.

In Tab. 1, the forward stepwise selection leading to model (22) is illustrated. The library functions in the expansion (2) consist of all polynomials of the position $\mathbf{q}$ and velocity $\dot{\mathbf{q}}$ up to order three. The first term included is the linear stiffness reducing the relative residual error to 0.6. Successively, nonlinear stiffness, external forcing, and linear damping are included in the identified model. The identification procedure is terminated once the relative residual error falls below 0.01. Some of the terms included in the function library, such as more complex damping terms of the form $\dot{q}^3$ and $q^2\dot{q}$, are not included in the final model.

Table 1: Overview of the forward stepwise selection that leads to model (22).

Iteration	1	2	3	4	5	6
Included term	q	q^2	q^3	$f^{(-1)}$	$f^{(1)}$	$\dot{q}$
Relative residual error	0.6	0.042	0.018	0.015	0.012	0.009

Omitted terms: $q\dot{q}$, $\dot{q}^2$, $q^2\dot{q}$, $q\dot{q}^2$, $\dot{q}^3$, $f^{(-2)}$, $f^{(2)}$.

In total, the identified model (22) has five parameters, which can all be related to physical sources. Linear and cubic stiffness terms have extensively been used to model magneto-mechanical oscillators similar to the experiment shown in Fig. 4 (cf., e.g., [8, 54, 82, 83]). This modeling is confirmed by the FrID algorithm. Quadratic stiffness terms are associated with asymmetries and in the magneto-mechanical oscillator shown in Fig. 4 asymmetries arise through, for example, asymmetric clamping of the cantilever and non-perfectly aligned magnets. A similar observation was also made in an earlier study of the same system [73]. Within the identification procedure, the asymmetry present in the data is automatically detected and modeled via a quadratic stiffness term.

Although damping is often nonlinear, it is macroscopically often modeled with linear damping terms. For the measurement data shown in Fig. 5a, the identification procedure confirms the linear damping hypothesis although more complex, nonlinear damping terms, for example, $\dot{q}^3$ or $q^2\dot{q}$, have been included in the function library for model (2) (cf. Tab. 1). The excitation is modeled as a single harmonic, although higher harmonics are included in Fourier expansion of the forcing function (4). However, these terms are eliminated within the simplification routine detailed in Section 2.4.3. Simulating the model (22) for forcing frequencies close to 40 Hz yields the forces response curve shown in Fig. 5b. Indeed, the simulated forced response of model (22) matches well with the measured forced response curve.

Moreover, it is worth discussing hyperparameters selected within FrID. To arrive at model (22), two Fourier modes are kept in the expansion ($K = 2$ in equation (5)), the threshold ε for the relative error tolerance is set to 0.01 (cf. Section 2.4.3), and polynomials of the position $\mathbf{q}$ and velocity $\dot{\mathbf{q}}$ up to order three are selected as library functions in the expansion (2). In the following, these hyperparameters are varied.

An increase in the number of Fourier modes K results in a larger linear system (15), and a higher number of parameters are required within FrID to minimize the fitting residual. Generally, this yields more complex models. For example, by increasing the number of harmonics K to three and keeping the error tolerance ε fixed, the nonlinear damping term $\dot{q}q^2$ and a second harmonic in the forcing function are automatically included in the identified model. The simulated force response curve of this more complex model closely reassembles the result shown in Fig. 5b. Furthermore, by keeping $K = 3$ and increasing the error tolerance ε to 0.011, one recovers a model of the form of equation (22). The same observations are made when the number of harmonics in the expansion (5) is increased beyond three ($K > 3$). This indicates the robustness of the identified model (22). For a single harmonic ($K = 1$), FrID is found to fail in identifying the quadratic nonlinearity in the model (22). This can be related to the fact that even powers of single-harmonic signals generate frequency content at even harmonics $K = 0, 2, 4, ...$, but not at the fundamental harmonic $K = 1$. Thus, even polynomials do not arise in equations (9) for $K = 1$, and even polynomials $g_p(\mathbf{q}, \dot{\mathbf{q}})$ are removed within the FrID algorithm. Hence, it is recommended to keep more than the fundamental harmonic in the expansion (5) to identify asymmetries.

Next, the degree of the utilized polynomials $g_p(\mathbf{q}, \dot{\mathbf{q}})$ in the expansion (5) is varied. If polynomials with a higher degree than three are included in the expansion (5), those terms are automatically removed by the

FrID algorithm, and hence, the same model (22) is obtained. If only second order polynomial and linear terms are included in the expansion (5), then FrID is found to fail in capturing the measured forced response. This is expected, since linear and quadratic models cannot capture the hardening behavior shown in Fig. 5a (cf., e.g., [8]). In practice, when utilizing a polynomial expansion (5), it is recommended to successively increase the degree of polynomials until no change in the model identified by FrID is observed.

Finally, the selection of the relative error tolerance ε (cf. Section 2.4.3) is discussed. Selecting a high threshold leads to an inaccurate model, while low values tend to result in overly complex models. To observe this behavior, the relative fitting residual is monitored during the forward stepwise selection procedure (cf. Section 2.4.3). The first term included in the model (22) is the linear stiffness, reducing the relative residual error to about 0.6. Then, the nonlinear stiffness terms are included in the model (22) reducing the relative residual error to a few percent. Subsequently, damping and forcing terms are identified. The remaining terms reduce the relative fitting residual only marginally (less than 0.01) indicating their insignificance. Generally, it is recommended to terminate the forward stepwise selection procedure, when the inclusion of additional terms only marginally reduces the residual error. For nonlinear structures such as the magneto-mechanical oscillator shown in Fig. 4, physical insights can also be employed to terminate the forward stepwise selection procedure. More specifically, models of nonlinear structures are expected to consist of terms from the following four categories: i) linear stiffness, ii) nonlinear stiffness, iii) damping, and iv) forcing terms. Hence, the forward stepwise selection can be terminated once a term from each of the four categories is found.

In Appendix A, the equation discovery tool SINDy [59] is utilized in an attempt to identify governing equations from the measurements shown in Fig. 5a. Herein, forced response data as well as additional resonance decay measurements are employed. Only the values of the linear stiffness and damping identified by SINDy are close to the values reported in equation (22). The nonlinear terms identified by the SINDy algorithm are more complex and cannot be related to physical effects. More crucially, the forced response measurements are not well captured by the SINDy models (cf. Fig. A.1 in Appendix A).

The unsuccessful attempts to utilize SINDy [59] prompt the authors to point out differences between SINDy and FrID. Primarily, SINDy is a time domain technique in which one seeks to minimize the modeling error at every time step whereas with FrID, one minimizes the fitting error in the frequency domain (cf. equation (9)). Additionally, the minimization procedures between FrID and SINDy differ and with FrID, one employs an explicit routine to reduce the effects of noise (cf. Section 2.4.1). Indeed, SINDy is known to be sensitive to noise and ensemble methods (Ensemble-SINDy) have been proposed to alleviate this shortcoming [60]. Therein, the SINDy algorithm is used to construct an ensemble of models, and subsequently the ensemble members are averaged. Unfortunately, this approach does not yield an improvement compared to the standard SINDy procedure for the measurements shown in Fig. 5a (cf. Appendix A).

The model (22) is further tested by verifying its extrapolation capabilities for different forcing amplitudes. There is often no a priori guarantee that identified models for a given excitation level can also yield meaningful results for other forcing amplitudes. Indeed, often in structural dynamics, it is found that models extrapolate poorly (e.g., [5, 32, 84]). This behavior can be a indication of overfitting to experimental data. Since the identified model (22) has only five parameters, an overfit seems unlikely. Moreover, it has been advocated [74] that sparsity is an ultimate regularizer in data-driven system identification that allows for better extrapolation and generalization capabilities. To verify this claim, the experiment is repeated for shaker control signals with different amplitudes. While the shaker control signal for the experiments shown in Fig. 5 has an amplitude of 1.5 V, forced response curves for excitation levels of 0.5 V, 1.0 V, and 2.0 V are measured. Then, simulations are carried out with the model (22) for the adjusted forcing amplitude values of $244.65 (= 733.96/1.5 \cdot 0.5)$, $489.31 (= 733.96/1.5 \cdot 1)$, and $978.61 (= 733.96/1.5 \cdot 2)$. The measurements and simulation results are included in Fig. 6.

Overall, the numerically computed forced responses match well with the experimental results, although some discrepancies are discernible. Especially, for the highest amplitude level and high amplitude responses, a mismatch between the numerically predicted and experimentally measured forced response curve is observed. The model (22) reaches its domain of validity and physical effects, not detectably present for the excitation level of 1.5 V are noticeable. The mismatch can be reduced by fitting a polynomial model to the measured response curve for the excitation level of 2.0 V. The resulting model is in the form of model (22) but the

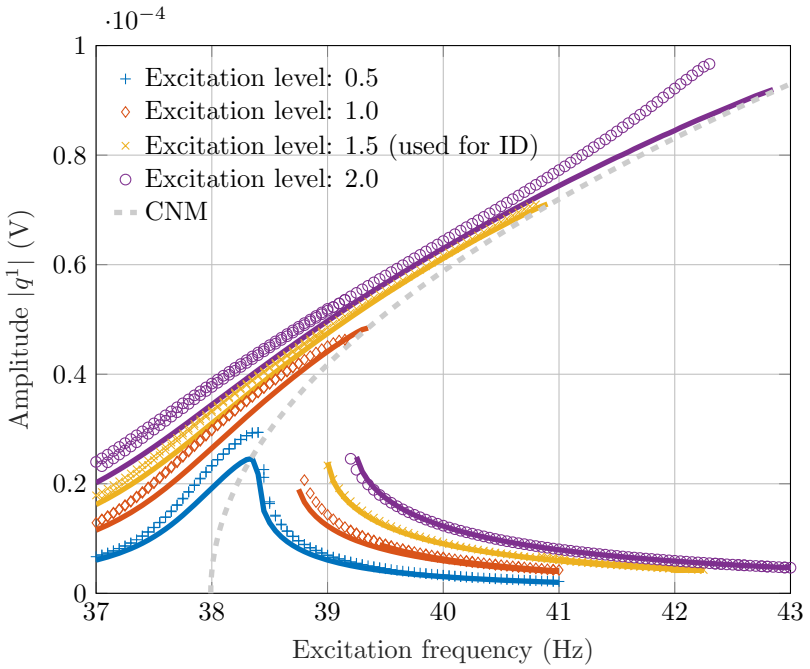

Figure 6: Single cantilever experiment: Simulated (solid lines), measured forced response curves (markers) and conservative nonlinear mode (CNM, gray dashed line).

parameter values are found to change. While the linear damping c, the linear stiffness k, and the forcing amplitude f remain almost unchanged, the quadratic stiffness term k_2 decreases to 7533.34 and the cubic stiffness k_3 increases to 20857.4.

Additionally, families of periodic orbits of the underlying conservative system can be computed from the obtained model (22). These families of periodic orbits, which are also denoted as nonlinear modes, have been extensively used to analyze the dynamics of nonlinear structures [30]. For example, their amplitude frequency dependency often aligns with the maxima of the forced response curve [85]. The conservative nonlinear modes are computed for the conservative and unforced part of the model (22), which is obtained by setting the damping c and excitation amplitude f to zero. The numerical continuation package COCO [80] is then utilized to compute the conservative nonlinear modes. The amplitude frequency relationship of the nonlinear modes of the conservative is included in Fig. 6. Except for the highest forcing level wherein the softening effect is not captured by model (22), the maxima of the forced response curves align well with the amplitude-frequency relationship of the conservative nonlinear mode. This further demonstrates the robustness and universality of the obtained model (22).

3.1.2. Multi-degree-of-freedom systems

After applying FrID to measurements obtained with a single mounted cantilever in the experiment shown in Fig. 4, the capabilities of FrID for the identification of multiple-degree-of-freedom systems are illustrated. To this end, two and three cantilevers are mounted in the experimental arrangement (cf. Fig. 4).

Small weights are added to the individual beams to detune their eigenfrequencies so that multiple distinct peaks are discernible in the frequency response shown in Fig. 7. In addition to the magnitude of the individual amplitudes $|q_j^1|$, the sums of the magnitude of the individual amplitudes are included in Fig. 7. In these curves, one can clearly discern two respectively three distinct peaks. The case of nearly identical beams resulting in a single peak in the frequency response (i.e., a structure with an internal resonance) is considered in the next section. Despite the detuning, the first eigenfrequencies of the cantilevers remain close. In the case of two cantilevers, the two response peaks are two Hz apart (approx. 5% of the eigenfrequencies), and in the case of

the three cantilevers, all three response peaks are located within 6 Hz (approx. 15% of the eigenfrequencies).

Coupling springs between adjacent cantilevers enhance the coupling between the oscillators. Indeed, for the two cantilever case, both strain signals q_1 and q_2 have a response maximum close to 41 Hz and a jump down is observed at 43.0 Hz (cf. Fig. 7a). Similarly, jumps at 36.6 Hz, 41.1 Hz, and 43.2 Hz are observable for all three cantilevers (cf. Fig. 7b). Due to this interaction, each resonance peak cannot trivially be fitted by using a single mode model, rather a model that can capture multiple modes simultaneously is necessary.

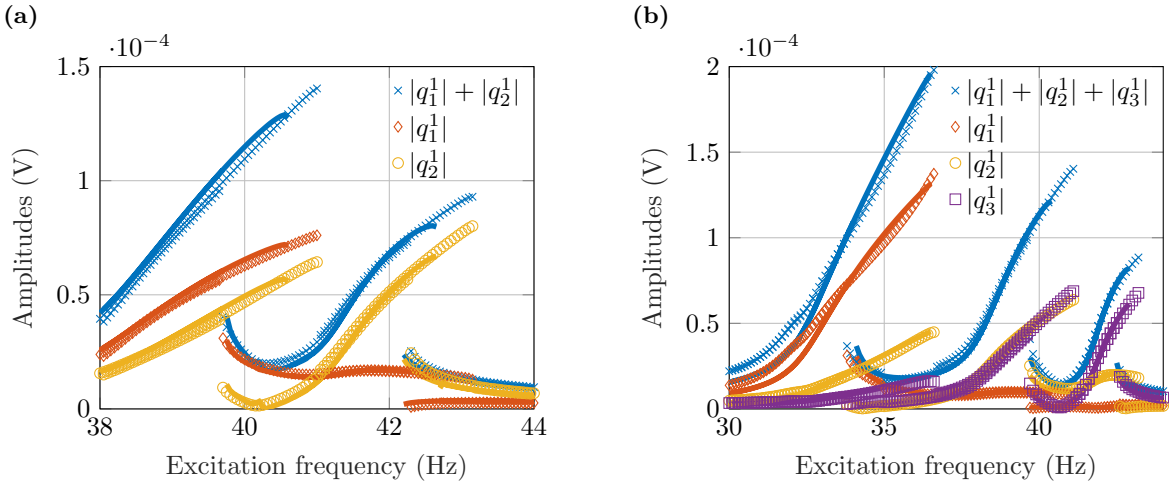

Figure 7: Multi-degree-of-freedom system: Measured (markers) and simulated forced response curves (solid lines). (a) Two cantilever system. (b) Three cantilever system.

For the two-cantilever system, the model

$$\begin{array}{llll} \ddot{q}_1 & +\eta_1 q_1^2 \dot{q}_1 & +k_1 q_1 + k_1^2 q_1^2 + k_1^3 q_1^3 + \nu_1 \dot{q}_1^2 q_1 & +k_{12} q_2 = f_1 \sin(\Omega t), \\ \ddot{q}_2 & +\eta_2 q_2^2 \dot{q}_2 & +k_2 q_2 + k_2^2 q_2^2 + k_2^3 q_2^3 + \nu_2 \dot{q}_2^2 q_2 & +k_{21} q_1 = f_2 \sin(\Omega t + \phi_2), \end{array} \tag{23}$$

is automatically identified by applying the FrID scheme. The numerical values are reported in Tab. 2 and the strain gauge signals have been non-dimensionalized with the constant $\alpha = 1.65 \cdot 10^{-4}$ V. The internal forces are approximated by polynomials of degree three, which results in 32 possible parameters in model (2). Only 12 of these parameters are included in the final model (23). In total, the model (23) is parameterized by 15 parameters.

Table 2: Identified parameters of the model (23) for the two-cantilever experiment shown in Fig. 7a.

DOF	damping	conservative terms				coupling	excitation	
	η_j	k_j	k_j^2	k_j^3	ν_j		f_j	ϕ_j
$j=1$	22.79	59943.65	18463.52	20413.45	-0.2	$k_{12} = -1994.98$	386.54	-
$j=2$	15.34	67166.37	4063	10243.7	-0.08	$k_{21} = -3957.4$	403.93	0.02

Similarly, for the three-cantilever system, with the FrID algorithm, the following model is automatically identified:

$$\begin{array}{llll} \ddot{q}_1 & +c_1 \dot{q}_1 & +k_1 q_1 + k_1^2 q_1^2 + k_1^3 q_1^3 + \nu_1 \dot{q}_1^2 q_1 & +k_{12} q_2 = f_1 \sin(\Omega t), \\ \ddot{q}_2 & +\eta_2 q_2^2 \dot{q}_2 & +k_2 q_2 + k_2^2 q_2^2 + k_2^3 q_2^3 + \nu_2 \dot{q}_2^2 q_2 & +k_{21} q_1 + k_{23} q_3 = f_2 \sin(\Omega t + \phi_2), \\ \ddot{q}_3 & +\eta_3 q_3^2 \dot{q}_3 & +k_3 q_3 + k_3^2 q_3^2 + k_3^3 q_3^3 + \nu_3 \dot{q}_3^2 q_3 & +k_{32} q_2 = f_3 \sin(\Omega t + \phi_3), \end{array} \tag{24}$$

The numerical values are reported in Tab. 3 and the strain gauge signals have been non-dimensionalized with the constant $\alpha = 2.93 \cdot 10^{-4}$ V. In model (24), the internal forces $\mathbf{N}(\dot{\mathbf{q}}, \mathbf{q})$ are parameterized by utilizing only 19 out of 83 possible parameters. Overall, the model (24) consists of 24 parameters.

Table 3: Identified parameters of the model (24) for the three-cantilever experiment shown in Fig. 7b.

DOF	damping		conservative terms				coupling	excitation	
	c_j	η_j	k_j	k_j^2	k_j^3	ν_j		f_j	ϕ_j
$j=1$	2.5	-	43678.86	9467.96	20879.32	-0.17	$k_{12} = -2950.2$	221.57	-
$j=2$	-	105.01	60666.38	38422.86	99154.94	-0.99	$k_{21} = -3644.6$ $k_{23} = -3180.9$	172.47	-0.05
$j=3$	-	55.97	67119.81	6913.4	38420.19	-0.33	$k_{32} = -5928.85$	219.55	-0.02

To obtain models (23) and (24) with the parameter values summarized in Tab. 2 and Tab. 3, three Fourier modes are kept in the Fourier expansion (5) ($K = 3$) and polynomials of order three are selected in the expansion (2). In Tab. 4 and 5 an overview of the forward stepwise selection procedures leading to the models (23) and (24) is provided. These hyperparameter choices are based on the heuristics detailed in Section 3.1.1. More specifically, the degree of the polynomials included in the expansion (2) is increased until a further increase in the degree of polynomials does not change the identified model, and the relative error threshold ε is selected so that the linear stiffness, nonlinear stiffness, damping, and forcing terms are included in the identified model. Furthermore, including more than three harmonics in the in the Fourier expansion (5) does not alter the models (23) and (24).

Table 4: Overview of the forward stepwise selection leading to model (23).

	Iteration	1	2	3	4	5	6	7	8
$j=1$	Included term	q_1	q_1^2	q_1^3	q_2	$\dot{q}_1^2 q_1$	$f_1^{(-1)}$	$q_1^2 \dot{q}_1$	$f_1^{(1)}$
	Relative residual error	0.123	0.092	0.064	0.044	0.034	0.03	0.026	0.02
$j=2$	Included term	q_2	q_2^3	q_1	q_2^2	$f_2^{(-1)}$	$f_2^{(1)}$	$\dot{q}_2^2 q_2$	$q_2^2 \dot{q}_2$
	Relative residual error	0.074	0.049	0.033	0.025	0.022	0.018	0.014	0.009

Table 5: Overview of the forward stepwise selection leading to model (24).

	Iteration	1	2	3	4	5	6	7	8	9
$j=1$	Included term	q_1	q_1^3	q_1^2	q_2	$\dot{q}_1^2 q_1$	$f_1^{(-1)}$	$f_1^{(1)}$	$\dot{q}_1$	-
	Relative residual error	0.127	0.091	0.062	0.050	0.044	0.04	0.037	0.035	-
$j=2$	Included term	q_2	q_1	q_2^2	q_2^3	q_3	$\dot{q}_2^2 q_2$	$f_2^{(-1)}$	$f_2^{(1)}$	$q_2^2 \dot{q}_2$
	Relative residual error	0.168	0.127	0.102	0.073	0.043	0.035	0.03	0.024	0.016
$j=3$	Included term	q_3	q_2	q_2^3	$f_3^{(-1)}$	$f_3^{(1)}$	q_3^2	$\dot{q}_3^2 q_3$	$q_3^2 \dot{q}_3$	-
	Relative residual error	0.099	0.063	0.040	0.034	0.027	0.019	0.015	0.01	-

A number of conclusions can be drawn from the identified models (23) and (24). Most importantly, both models consist of linear, quadratic, and cubic stiffness terms. This is expected, since the same observation

has also been made for the single cantilever experiment (cf. Section 3.1.1) and the captured physical effects remain the same. Additionally, internal forces proportional to $\dot{q}_j^2 q_j$ arise for all coordinates. While the origin of these terms is unclear, they are conservative as they could arise through a position dependent mass matrix.

The connecting springs between the oscillators are automatically identified as linear spring coefficients and the spring coupling between only neighboring oscillators is correctly predicted. More specifically, the coefficients k_{ji} ($j \neq i$) in the identified models (23) and (24) indicate coupling between the j-th cantilever and the i-th cantilever. The coefficients k_{12} and k_{21} account for coupling between the first and the second cantilever, whereas the parameters k_{23} and k_{32} correspond to coupling between the second and third coordinates in equation (24). Moreover, the first coordinate of the three degree-of-freedom model (24) is not coupled to the third coordinate. This coupling topology corresponds to the coupling springs added in the experiment (cf. Fig. 4) and is automatically identified purely from experimental measurements. It is noted that the coupling spring coefficients are not symmetric (cf. $k_{12} \neq k_{21}$ and $k_{23} \neq k_{32}$ in Tab. 2 and 3). This observation is not in contradiction with the fact that stiffness matrices in mechanics are commonly symmetric and positive definite. As pointed out earlier, the model (1) is formulated in a set of coordinates so that the mass matrix is the identity matrix. Indeed, different masses attached to the cantilevers in the experiments (cf. the right cantilever in Fig. 4) give rise to a non-symmetric matrix $\mathbf{M}^{-1}\mathbf{K}$.

The identified damping is primarily nonlinear, with the exception of the first coordinate in the three-cantilever experiment (24). Damping remains a nonlinear effect [30], which is challenging to identify and often simply assumed to be linear. With the considered multi-degree-of-freedom examples, the linear damping hypothesis is overwhelmingly rejected, and nonlinear damping is found to describe the measured response curves more accurately. The underlying physical effects of this particular damping remain to be explored.

Simulating the responses of systems (23) and (24) with the parameters given in Tab. 2 and Tab. 3 yields the response curves shown in Fig. 7. Overall, the forced response is accurately captured with the identified models.

3.1.3. Structure with internal resonance

Structures with internally resonance continue to pose a challenge to many competing system identification procedures [15–17, 34, 36], as a single active mode of vibration in these procedures is implicitly assumed. However, the response of a system with an internal resonance cannot be approximated by using a single isolated mode. On the other hand, no such assumption is made within FrID. Therefore, one can capture modal interactions. To demonstrate this capability, a system with an internal resonance is investigated. In practice, internal resonances often arise due to underlying symmetries present in many structures.

The frequency response curves of two cantilevers with approximately equal eigenfrequencies are shown in Fig. 8. Depending on the excitation frequency, one, two, three, or four different steady state vibrations are observed. Apart from the main branch, two isolated response branches are observed. Along these isolated modes, one cantilever vibrates with a high amplitude, whereas the other cantilever vibrates with a significantly lower amplitude. Due to this energy confinement, such response patterns have also been described as localized modes [86–88], and recently, the effects of noise on such localized modes have been studied [89]. Experimentally, the isolated localized modes are realized by manual perturbations. More specifically, high amplitude vibrations on the main branch with 39.5 Hz are realized and then one of the cantilevers is perturbed manually, which triggers the corresponding beam to vibrate with a lower amplitude. This procedure realizes a localized mode. The remaining branch of the localized mode is then obtained by sweeping up or down.

Selecting the same hyperparameters as detailed in Section 3.1.2, with FrID, one identifies exactly the same form of model as the model (23) in Section 3.1.2, despite the more intricate frequency response curve shown in Fig. 8. This similarity is expected, as the two experimental systems are similar with the same underlying physical effects. However, the utilized cantilevers, connecting springs, and added masses differ; therefore, the identified parameter values change. The numerical values for the system with the internally resonance are listed in Tab. 6 and the strain gauge signals have been non-dimensionalized with the constant $\alpha = 1.82 \cdot 10^{-4}$ V. The linear eigenfrequencies are 37.54 Hz and 37.36 Hz, which indicates a 1:1 frequency relationship. In Tab. 7, the authors provide an overview of the model selection procedure leading to the final model (23) with the parameters summarized in Tab. 6.

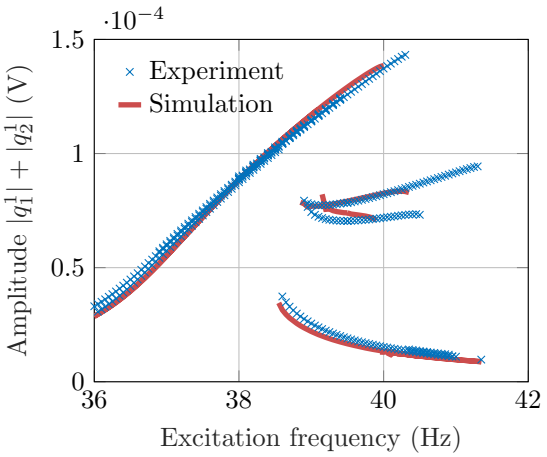

Figure 8: Forced response curves of a structure with a one-to-one internal resonance.

Table 6: Identified parameters of the model (23) for the internal resonance case 8.

DOF	damping	conservative terms				coupling	excitation	
	η_j	k_j	k_j^2	k_j^3	ν_j		f_j	ϕ_j
$j=1$	17.17	55631.64	-	20991.87	-0.14	$k_{12}=-904.55$	340.22	-
$j=2$	29.06	55092.26	9802.31	31607.74	-0.29	$k_{21}=-518.47$	273.87	-0.01

Table 7: Overview of the forward stepwise selection leading to the identified parameters of the model (23) for the internal resonance case 8.

	Iteration	1	2	3	4	5	6	7	8
$j=1$	Included term	q_1	q_1^2	q_1^3	$\dot{q}_1^2 q_1$	q_2	$f_1^{(-1)}$	$q_1^2\dot{q}_1$	$f_1^{(1)}$
	Relative residual error	0.131	0.093	0.035	0.029	0.027	0.024	0.022	0.018
$j=2$	Included term	q_2	q_2^3	q_2^2	$\dot{q}_2^2 q_2$	q_1	$f_2^{(-1)}$	$q_2^2\dot{q}_2$	$f_2^{(1)}$
	Relative residual error	0.097	0.062	0.038	0.028	0.024	0.021	0.017	0.011

As in the experiments, additional steps are required to capture the isolated branches of the forced response curves with numerical simulations. Similar to the experimental procedure, an initial condition on the main branch with high amplitude vibrations at 39.5 Hz is selected, and then, the initial position of one of the degrees-of-freedom is perturbed numerically. This perturbation causes the corresponding response coordinate to oscillate with a lower amplitude, and thereby, one realizes a localized mode. The remaining branch of the localized mode is then obtained by successively increasing or decreasing the excitation frequency. Many competing system identification procedures for nonlinear systems rely on a single mode approximation and they cannot be applied to the response data shown in Fig. 8. On the other hand, by using FrID, an accurate and simple model is identified. As shown in Fig. 8, the simulated forced response of the model (23) with the identified parameters listed in Tab. 6 matches well with the experimentally observed forced response.

3.2. Clamping nonlinearities

To further illustrate the universality of FrID, this scheme is applied to the data from the experiment shown in Fig. 4 without magnets. While in the previous experiments, the attached magnets significantly impact the force-deflection curve of the cantilevers, two magnets have been removed for the experiments discussed in this section (cf. Figure 9a)[6]. The measured forced response curves are shown in Fig. 9b. Therein, it is observed, that the frequency at which the maximal response amplitude occurs changes with the excitation level. This characteristic can only be observed for nonlinear structures.

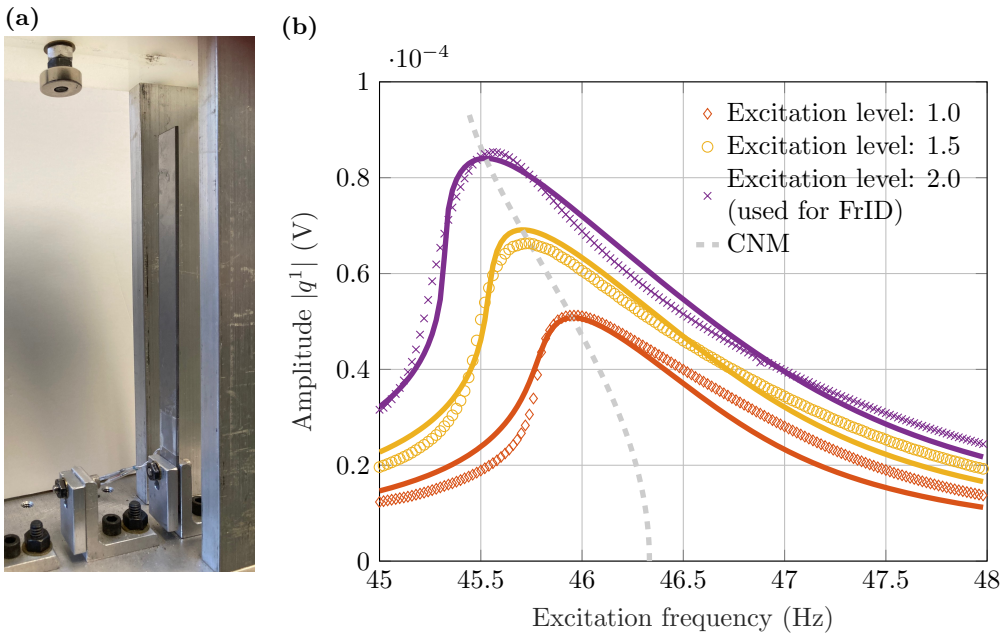

Figure 9: Clamping nonlinearities: (a) Mounted cantilever without magnets at the tip and on the opposite side at the frame. (b) Measured (markers) and simulated (solid lines) forced response curves as well as the conservative nonlinear mode (CNM, dashed gray line).

After applying FrID to the forced response curve with the maximal excitation level, the result is the oscillatory system

$$\ddot{q} + c\dot{q} + \nu q^2\dot{q} + kq + k_3q^3 + k_5q^5 = f\cos(\Omega t), \tag{25}$$

with the parameters

$$c = 4.2 \qquad \nu = 7.13, \qquad k = 84748.84, \qquad k_3 = -6042.78, \qquad k_5 = 2424.39, \qquad f = 821.77, \tag{26}$$

wherein the strain gauge signals have been non-dimensionalized by dividing with the constant $\alpha = 1.7266 \cdot 10^{-4}$ V. To this end, polynomials of order five are included in the expansion (2), the error tolerance ε is set to 0.5%, and three harmonics are kept in the Fourier expansion (5) within the FrID algorithm. Moreover, in Tab. 7, the authors provide an overview of the model selection procedure leading to the final model (25) with the parameter values (26).

The simulated forced response curves are shown in Fig. 9b. For the excitation level of 1.0 V, the forcing amplitude f is set to 410.89(= 821.77/2) and for the excitation level of 1.5 V, the forcing amplitude is set to 616.33(= 821.77/2 · 1.5). The forced response curves obtained from the simulations are found to agree

[6]Admittedly, this experiment stems from an attempt to first verify FrID's performance with response measurements of a linear oscillator.

Table 8: Overview of the forward stepwise selection leading to model (25).

Iteration	1	2	3	4	5	6	7
Included term	q	q^3	$f^{(-1)}$	$f^{(1)}$	$\dot{q}$	$q^2\dot{q}$	q^5
Relative residual error	0.03	0.021	0.018	0.014	0.007	0.005	0.005

Omitted terms: q^2, $q\dot{q}$, $\dot{q}^2$, $\dot{q}^2q$, $\dot{q}^3$, q^4, $q^3\dot{q}$, $q^2\dot{q}^2$, $q\dot{q}^3$, $\dot{q}^4$, $q^4\dot{q}$, $q^3\dot{q}^2$, $q^2\dot{q}^3$, $q\dot{q}^4$, $\dot{q}^5$.

well with the measurements. Moreover, conservative nonlinear modes for the model are calculated with the continuation package COCO [80]. These nonlinear modes align well with the response maxima, which further illustrates the universality and extrapolation capabilities of the identified model (25).

The frequency at which the maximal response occurs decreases with increasing excitation level (cf. Fig. 9b). Between the excitation levels 1.0 V and 1.5 V, the response peak shifts by approximately 0.3 Hz whereas from 1.5 V to 2.0 V, a shift by only 0.1 Hz is observed. Thus, the softening trend decreases at higher amplitudes. This behavior is denoted as softening-hardening characteristics and is also observed in similar experiments (e.g., [90, 91]). The initial softening can be related to micro-slip in the bolts [92, 93], whereas the hardening could stem from geometric effects of beam bending [8]. Although this softening-hardening behavior is directly not discernible from a single response curve, with FrID, one remarkably identifies a model accurately reproducing this characteristic from a single response curve. In the model (25), the negative cubic spring coefficient k_3 captures the initial softening, and a positive quintic spring coefficient k_5 captures the hardening behavior at higher amplitudes.

The main source of the damping in the experimental arrangement shown in Fig. 9a is the clamp. While it could be idealized as a clamped boundary, a characterization as a bolted joint is more realistic. Bolted joints generally induce nonlinear damping effects, which are accurately captured in the model (25). The FrID scheme includes the linear damping coefficient c and a nonlinear damping of the form $q^2\dot{q}$. Also, in the experiments with attached magnets from the previous Section 3.1, either linear or nonlinear damping terms of the form $q^2\dot{q}$ are included (cf. the models (22), (23), and (24)). Hence, it can be concluded that the damping is most accurately described by including both terms. In some experiments, the effects of the linear or the nonlinear damping term are negligible, and thus, the corresponding term is eliminated during the identification process.

3.3. Joint nonlinearities

As a final demonstration, the FrID scheme is applied to the external data set [78] containing response measurements of a structure with a bolted joint. The application of FrID to this external data set further illustrates the universality and flexibility of the proposed identification routine.

Many engineering structures feature joints and often these joints have a severe impact on the structure's dynamics [94–96]. This importance motivates many researchers to investigate jointed structures. Amongst them, Jin *et al.* [90] perform a series of shaker experiments on a structure, which consists of two beam halves jointed together by three bolts (cf. Figure 10a). The assembly is 28.35 inches long, 0.5 inches thick, and 1 inch wide. This experimental set-up is a modification of a beam investigated by Brake, Schwingshackl, and Reuss [97] and more details can be found in the associated literature [90, 98]. The published free response data [78] has been extensively used for system identification, whereas the forced response data has been less studied. To the best of the author's knowledge, no equations of motion have been identified.

The external measurements [78] have a number of differences compared to the response data utilized in the previous sections (Sections 3.1 and 3.2). Most importantly, the data [78] contains only measurements of the first harmonic. Hence, only those data can be employed for fitting and the Fourier expansions (4), (6), and (7) are terminated after one term retaining only the equations for $K = 1$ and $K = -1$. Moreover, polynomials up to a degree of five are kept in the expansion (2) and the error tolerance ε is set to 0.15%. On application of the FrID scheme to the forced response curves [78], the result is the model

$$\ddot{q} + cq + \nu q^2\dot{q} + kq + k_3q^3 + k_5q^5 = \beta f\cos(\Omega t), \tag{27}$$

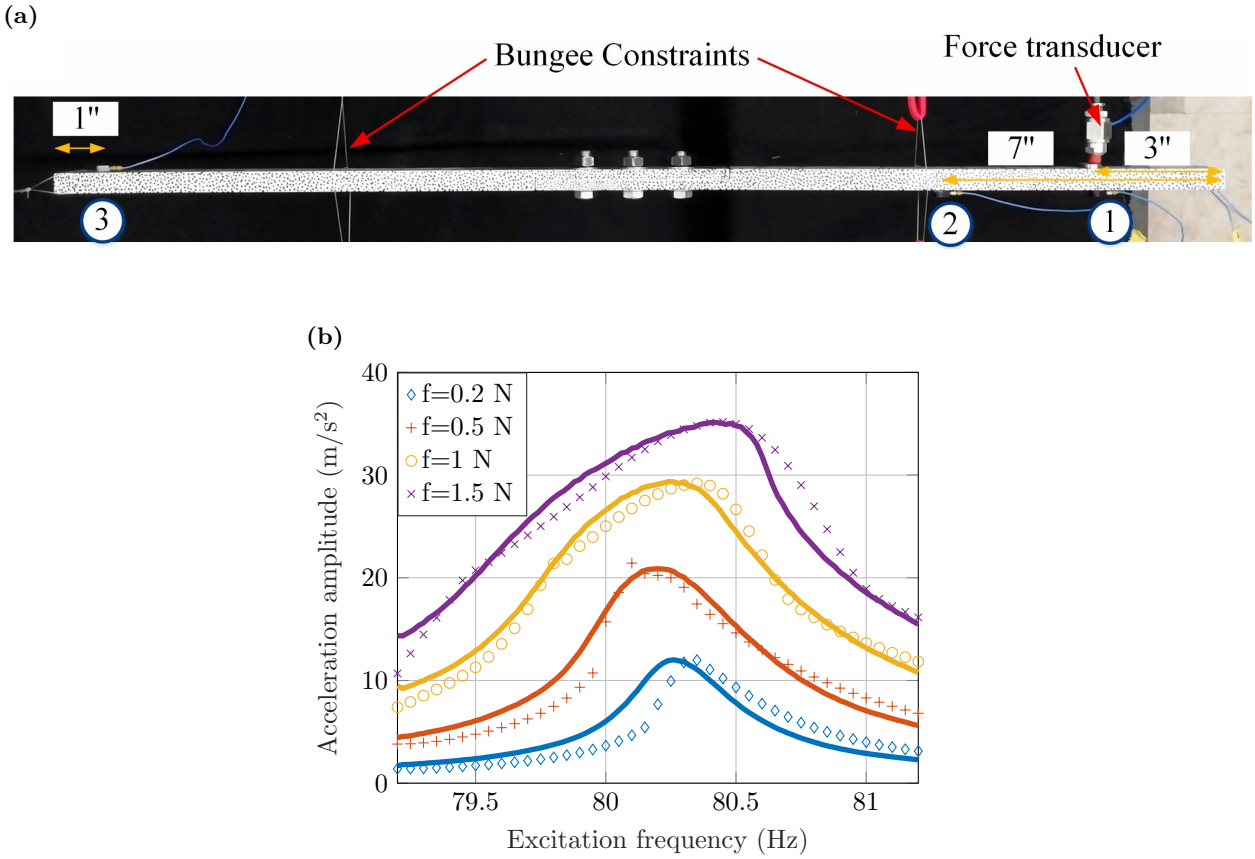

Figure 10: System with joint nonlinearities: (a) Experimental set-up* (b) Measured (markers) and simulated (solid lines) forced response curves.
* Figure reprinted from [98], with permission from Elsevier.

with the parameters

$$\begin{aligned} &c = 1.63 \text{ Ns/(kg m)}, && \nu = 2 \cdot 10^8 \text{ Ns/(kg m}^3\text{)}, && \beta = 0.5 \text{ 1/kg}, \\ &k = 2.55 \cdot 10^5 \text{ N/(kg m)}, && k_3 = -6.69 \cdot 10^{10} \text{ N/(kg m}^3\text{)}, && \kappa_5 = 4.63 \cdot 10^{21} \text{ N/(kg m}^5\text{)}, \end{aligned} \tag{28}$$

which are all mass normalized[7]. The forward stepwise selection procedure is summarized in Tab. 9. It is noted that the model of the beam with joint nonlinearities (27) corresponds to the identified model for the earlier investigated clamped beam (25). This agrees with the expectation that similar physical effects, softening-hardening behavior and nonlinear damping, give rise to the same functional form. Of course, the individual parameters are found to differ (cf. equation (28) and equation (26)).

The simulated forced response curves are found to capture the measured response curves well. Some discrepancies for the highest and lowest forcing amplitudes are noticeable. These differences can be related to two facts. First, within the numerical simulations, the forcing amplitude was kept constant according to the nominal values ($f = 0.2, 0.5, 1, 1.5$ N), whereas in reality, the forcing amplitudes are not constant and vary up to 30 %. Furthermore, only the amplitudes and phases of the first harmonic are available for

[7]With the modal mass of $m = 1.55$ kg reported in [90], the equation (27) and the parameter values (28) can be rewritten such that equation (27) is a force balance equation.

Table 9: Overview of the forward stepwise selection leading to model (27).

Iteration	1	2	3	4	5	6	7
Included term	q	$f^{(-1)}$	$f^{(1)}$	$q^2\dot{q}$	$\dot{q}$	q^5	q^3
Relative residual error	0.01	0.008	0.006	0.003	0.002	0.002	0.001

Omitted terms: q^2, $q\dot{q}$, $\dot{q}^2$, $\dot{q}^2q$, $\dot{q}^3$, q^4, $q^3\dot{q}$, $q^2\dot{q}^2$, $q\dot{q}^3$, $\dot{q}^4$, $q^4\dot{q}$, $q^3\dot{q}^2$, $q^2\dot{q}^3$, $q\dot{q}^4$, $\dot{q}^5$.

fitting. With such data, the FrID scheme cannot be used to identify even polynomials (e.g., q^2, $\dot{q}q$, or $\dot{q}^2$), which could, however, be present. Incorporating richer measurements could enhance the accuracy of the fit further. Nevertheless, the simple and interpretable model (27) accurately captures the forced response data (cf. Fig. 10b).

As an alternative to FrID, the recently introduced data-driven system identification tool SSMLearn [99] could be employed to derive a model for the forced response of the jointed structure. However, as the developers of this algorithm admit, SSMLearn is limited to weak forcing, and currently, cannot model the forced response data of the jointed structure shown in Fig. 10 [100]. On the other hand, the FrID-model (27) can be used to accurately capture the forced response data [78] (cf. Fig. 10b).

4. Concluding Remarks

In this article, an automated identification procedure to determine sparse governing equations of nonlinear oscillators from forced response measurements has been presented and experimentally validated. The approach relies on an expansion of steady state measurements in the frequency domain and an approximation of the internal forces with an abundance of library functions (cf. equation (2)). As a result, one obtains equations linear in the unknown parameters, which can be found by minimizing the least squares residual. To increase the robustness, extrapolation capabilities, and interpretability of the obtained equations, three essential steps are performed. First, the noise floor is estimated from the measurements and coefficients below the noise floor are truncated. Subsequently, approximate linear dependencies are removed, and only terms reducing the residual significantly are included in final equations of motion. Within these steps the abundance of library functions is reduced and spurious terms from the identified equations of motion are removed. As a result, this procedure yields basic and robust governing equations of nonlinear oscillators.

All aforementioned steps are assembled in the automated MATLAB package FrID[8], which is then applied to a variety of forced response measurements. In these experiments, geometry, as well as, magnets (cf. Section 3.1), clamps (cf. Section 3.2), and joints (cf. Section 3.3) induce nonlinearities. Additional to single-degree-of-freedom systems, two- and three-degree-of-freedom systems, including one with an internal resonance are considered. For all these systems, the FrID scheme is found to be reliable in identifying robust and interpretable governing equations. The simulated forced response curves of these models match well with the measured steady state responses. For the obtained measurements, the FrID scheme is found to outperform the competing equation discovery tools SINDy [59] and SSMLearn [99]. Thus, the developed scheme opens up the opportunity to reliably identify nonlinear oscillators from frequency response measurements, and thereby, provides a robust basis to extend modal testing to nonlinear structures.

The FrID scheme can only benefit from application to as many forced response measurements as possible. Such applications could in turn inspire, for example, alternative simplification routines (cf. Section 2.4.3), weighted norms for the least squares fit and other application specific modifications. Structures with stops or clearances could be an interesting application for FrID. Since such systems are commonly modeled by utilizing non-smooth functions, it will be crucial to assess the capabilities of polynomials to fit the forced response, and possibly, include more appropriate library functions in the model (2). Moreover, joints and

[8]FrID is publicly available at `https://github.com/tbreunung/FrID`.

friction phenomena often require considerable modeling efforts. The macroscopic effects of such phenomena can be captured with the FrID algorithm, which is found to yield basic, data-driven reduced order models.

Similarly, application of FrID to more structures with multiple nonlinear resonances is a natural continuation of this work. Within this article, applications to structures with two and three closely spaced resonances as well as a structure with an internal resonance are presented. The models obtained through the FrID scheme are found to accurately capture the forced response of the underlying structure and include coupling between the modes. Additional structures with multiple internal resonances could be considered as well.

To the best of the authors' knowledge, the FrID scheme is the first system identification tool for nonlinear oscillators based on a sparse regression in the frequency domain. While it is demonstrated that this approach has advantages compared to an approach based on regression in the time domain (i.e. SINDy [59] and its variants [60]) for the frequency response measurements obtained in this article, it is anticipated that time-domain-based identification routines can be improved and that both approaches would offer unique advantages for individual applications. Similar to modal testing for linear structures [1, 7, 69], a mutual coexistence of methods based in the frequency domain and the time domain is expected.

The presented system identification procedure is a black-box, data-driven approach, which, to a large extent, is agnostic to the underlying physical aspects such as sensor location, exciter location, and exciter input in the test set-up. Of course, this black-box, data-driven approach can only yield meaningful models if the supplied measurement data is rich enough to characterize the observed dynamics. While this is the case for the experiments utilized in this article, in practice, sensor type, sensor placement, data-acquisition system, and excitation location need careful consideration. While some guidelines are available for linear modal analysis [7], less experience is available for nonlinear structures. All these aspects remain important research directions for the identification of nonlinear structures.

Moreover, in this article, it is assumed that one measurement channel is available for each generalized coordinate. The cases of abundant measurements (more measurements than coordinates/modes) and sparse sensors (less measurements than coordinates/modes) could be considered in the future. Additional measurements could be used for cross-validation to further improve the robustness of the obtained model, whereas sensor placement for sparse measurements could be a further topic for research. Finally, the number of degrees of freedom required to capture the structure's nonlinear forced response needs to be obtained from measurements, as it is commonly done for linear structures by using stabilization diagrams.

Acknowledgements.. The authors gratefully acknowledge the support of the National Science Foundation through Grant no. CMMI 1760366, the support from the Minta Martin Professorship, and the opportunity to present a selection of the presented results at the International Modal Analysis Conference XLI in Austin, TX [101] and receive feedback. Moreover, the authors are thankful to Matt Allen for encouraging discussion of this work at an early stage and to Gelb Kleyman, Sebastian Tatzko, Matthew Brake, Cengizhan Taslicay, Meghan Shemer, Jae Min You, and Lautaro Cilenti for supplying additional measurements for verification (not included in this article).

Conflict of Interest

The authors have no conflicts to disclose.

Data availability

The MATLAB script FrID along with all measurements recorded for this manuscript is publicly available at `https://github.com/tbreunung/FrID`. The measurements for Section 3.3 are available at [78].

Author contributions

Thomas Breunung: Conceptualization, Methodology, Software, Validation, Formal analysis, Investigation, Data Curation, Writing - Original Draft. **Balakumar Balachandran**: Conceptualization, Methodology, Writing- Review & Editing, Supervision, and Funding acquisition.

A. Applying the SINDy algorithm [59] for single degree-of-freedom system studied in Sect. 3.1.1

The equation discovery tool SINDy [59] can be applied to first order systems of the form

$$\dot{\mathbf{x}} = \mathbf{f}(\mathbf{x}) = \sum_{p=1}^{P} \mathbf{N}^p g_p(\mathbf{x}). \tag{A.1}$$

As equation (A.1) indicates, SINDy [59] also relies on expansion of the unknown dynamics through a set of library functions similar to the expansion in equation (2) and subsequent regression promoting sparsity of the fitted equations. To utilize SINDy for the forced response data from Section 3.1.1, external periodic forcing is added to model (A.1), resulting in

$$\dot{\mathbf{x}} = \mathbf{f}(\mathbf{x}) = \sum_{p=1}^{P} \mathbf{N}^p g_p(\mathbf{x}) + \sum_{k=1}^{K} \left(\mathbf{f}_s^{(k)} \sin(\Omega t) + \mathbf{f}_c^{(k)} \cos(\Omega t) \right). \tag{A.2}$$

With this modification, SINDy has the same set of basis functions as FrID and the transformation $\mathbf{x} = [q, \dot{q}]^\top$ transform model (1) into system (A.2). It is noted that SINDy requires the knowledge of the velocities and accelerations, which are not recorded in the experiments of Section 3.1.1. To this end, the positions measurements are transformed into the frequency domain (cf. equation (6)) to recover the time series of the acceleration and the velocity. With the choice of the sparsity promoting parameter $\lambda = 0.01$, the SINDy algorithm is found to yield the equations

$$\begin{aligned} \dot{x}_1 &= x_2 \\ \dot{x}_2 &= -64033.56x_1 - 3.25x_2 - 27910894.52x_1^2 + 3168.43x_1x_2 + 412.05x_2^2 + 10964647.35x_1x_2^2 + 5457.6x_2^3 \\ &\quad - 0.048\sin(\Omega t) \end{aligned} \tag{A.3}$$

The SINDy algorithm successfully recovers the second order nature of the supplied data (cf. the first line of equation (A.3)) and also the values of the identified linear stiffness and damping coefficients are close to the values identified by FrID (cf. equation (22)). The linearized eigenfrequency of system (A.3) is approximately 40.3 Hz and within the frequency range expected from the experimental data (cf. Fig. 5a). However, some of the nonlinear terms identified by SINDy are difficult to relate to physical sources (e.g., the term $x_1x_2 = q\dot{q}$) and the SINDy-model (A.3) consists of more nonlinear terms than the FrID-model (22). To yield a sparser model, the SINDy-parameter λ can to be increased. However, the first coefficient that would be removed is the external forcing, when λ exceeds 0.048. This yields an unforced system with the trivial forced response $\dot{q} = q = 0$. A simulation of the forced response of system (A.3) yields the forced response curve included in Fig. A.1a (cf. SINDy with decay data). The computed forced response does not match the experimentally observed response. The main branch of the simulated forced response has significantly smaller amplitudes than the measured values, and close to resonance, large jumps to amplitudes four times higher than the measured values are predicted.

Attempts to increase the accuracy of the fit by allowing for more parameters in the SINDy algorithm were unsuccessful. For example, decreasing the tuning parameter λ yields models with more nonlinear terms than equation (A.3). However, the additionally included terms are small and no change of the simulated response is observed. Moreover, increasing the degree of polynomials in SINDy's library of nonlinear functions yields models for which the forced response escapes to infinity for the simulated sweeps.

An additional identification with the SINDy algorithm is attempted by utilizing resonance decay measurements (e.g., [102]). Therein, a shaker is utilized to excite the nonlinear structure close to a resonance maximum. Then, the excitation source is turned off and the arising free decay measurements are recorded. The autonomous SINDy-model (A.1) can be utilized for this type of data. In a second step, periodic excitation is added to the SINDy-model to compare the results to the forced response measurements included in Section 3.1.1.

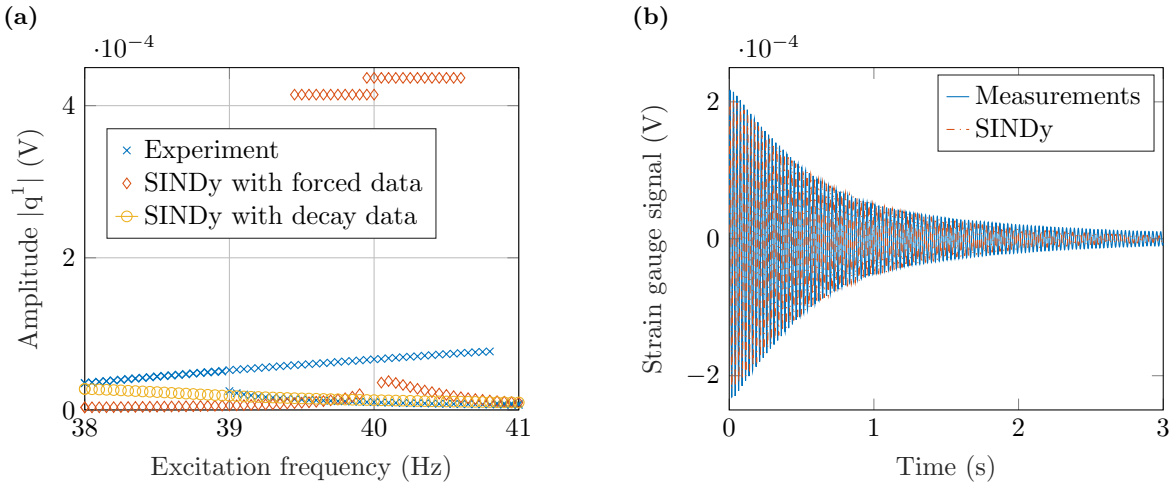

Figure A.1: Comparison with SINDy for the single degree-of-freedom system from section: (a) Measured and simulated forced response curves. (b) Resonance decay measurements and fit obtained with SINDy.

For the single degree-of-freedom system from Section 3.1.1, the excitation level of 2.0 is selected to ensure that the vibrations amplitudes shown in Fig. 5a are within the amplitude range of the resonance decay. Then, the high amplitude vibrations close to 42.0 Hz are realized, the shaker is turned off, and the decaying response is measured. This resonance decay measurement is shown in Fig. A.1b. When this data is used with the SINDy algorithm, one obtains the system

$$\begin{aligned}\dot{x}_1 &= x_2,\\ \dot{x}_2 &= -5.35\cdot 10^4 x_1 - 2.38 x_2 - 3.07\cdot 10^7 x_1^2 - 1.25\cdot 10^4 x_1 x_2 - 152.92 x_2^2 - 2.89\cdot 10^{11} x_1^3 + 5.06\cdot 10^7 x_1^2 x_2\\ &\quad - 8.56\cdot 10^6 x_1 x_2^2 - 2.8\cdot 10^3 x_2^3 + 4.51\cdot 10^9 x_1^2 x_2^2 + 8.5\cdot 10^6 x_1 x_2^3 + 2.3\cdot 10^4 x_2^4 + 1.43\cdot 10^9 x_1 x_2^4 + 1.12\cdot 10^6 x_2^5.\end{aligned} \tag{A.4}$$

To achieve an accurate fit with the resonance decay measurements, polynomials of up to order five need to be included in SINDy's library of nonlinear functions. Similar to the forced case, the values of the linear stiffness and damping coefficients are close to the values identified with FrID (cf. equation (22)). However, the nonlinear terms identified by SINDy are significantly more complex than the terms included in equation (22).

To emulate a forced response, single harmonic forcing is added to the second coordinate of equation (A.4) and the forced response is simulated. The forcing amplitude was selected so that the amplitudes of the simulations and measurements match for an excitation frequency of 38.0 Hz. This simulated forced response is shown in Fig. A.1a (cf. SINDy with decay data). While the low amplitude branch is captured, the resonance peak and the high amplitude branch are completely missed. Attempts to increase the accuracy of the simulated forced response by including more or less polynomials in SINDy's library of nonlinear functions or a variation of the specific parameter λ did not yield a system with a forced response curves that match the measurement better than equation (A.4).

The task of identifying a system from free decay measurements and then predicting a forced response is an extrapolation (from unforced measurements to forced response). This is generally a more challenging task than fitting on the same forced response measurements as done when obtaining the SINDy-model (A.3) or the FrID-model (22). In either case, starting from forced response data or resonance decay measurements, both SINDy-models (A.3) and (A.4) do not capture measured forced response (cf. Fig. A.1a).

In a final attempt, the Ensemble-SINDy algorithm [60] is applied to the forced response measurements from Section 3.1.1 and the decay measurement shown in Fig. A.1b. With Ensemble-SINDy, an ensemble of

models are constructed by utilizing a bootstrapping technique and subsequent application of the standard SINDy-algorithm. A final model is then obtained by taking the mean of median of coefficients of the identified models. Unfortunately, this approach does not result in any major changes compared to results obtained with the standard SINDy-algorithm. While the parameter values reported in the equations (A.3) and (A.4) change slightly, the functional form of the equations equations (A.3) and (A.4) (i.e., the identified terms) remains the same and, more crucially, the results shown in Fig. A.1 do not change. Thus, the ensemble techniques proposed in [60] are found to be not sufficient to identify an accurate model for single degree-of-freedom system studied in Sect. 3.1.1.

References

[1] D. J. Ewins, Modal testing: theory, practice and application, John Wiley & Sons, 2009.

[2] S. Billings, K. Tsang, Spectral analysis for non-linear systems, part i: Parametric non-linear spectral analysis, Mechanical Systems and Signal Processing 3 (4) (1989) 319–339. doi:10.1016/0888-3270(89)90041-1.

[3] M. Feldman, Non-linear system vibration analysis using hilbert transform–i. free vibration analysis method'freevib', Mechanical Systems and Signal Processing 8 (2) (1994) 119–127. doi:10.1006/mssp.1994.1011.

[4] J. M. Londoño, S. A. Neild, J. E. Cooper, Identification of backbone curves of nonlinear systems from resonance decay responses, Journal of Sound and Vibration 348 (2015) 224–238. doi:10.1016/j.jsv.2015.03.015.

[5] M. Scheel, G. Kleyman, A. Tatar, M. R. Brake, S. Peter, J.-P. Noël, M. S. Allen, M. Krack, Experimental assessment of polynomial nonlinear state-space and nonlinear-mode models for near-resonant vibrations, Mechanical Systems and Signal Processing 143 (2020) 106796. doi:10.1016/j.ymssp.2020.106796.

[6] M. Wall, M. S. Allen, R. J. Kuether, Observations of modal coupling due to bolted joints in an experimental benchmark structure, Mechanical Systems and Signal Processing 162 (2022) 107968. doi:10.1016/j.ymssp.2021.107968.

[7] P. Avitabile, Modal testing: a practitioner's guide, John Wiley & Sons, 2017. doi:10.1002/9781119222989.

[8] A. H. Nayfeh, D. T. Mook, Nonlinear oscillations, John Wiley & Sons, 2008. doi:10.1002/9783527617586.

[9] J. Guckenheimer, P. Holmes, Nonlinear oscillations, dynamical systems, and bifurcations of vector fields, Vol. 42, Springer Science & Business Media, 2013. doi:0.1007/978-1-4612-1140-2.

[10] A. H. Nayfeh, B. Balachandran, Applied nonlinear dynamics: analytical, computational, and experimental methods, John Wiley & Sons, 2008. doi:10.1002/9783527617548.

[11] M. P. Castanier, C. Pierre, Using intentional mistuning in the design of turbomachinery rotors, AIAA Journal 40 (10) (2002) 2077–2086. doi:10.2514/2.1542.

[12] M. P. Castanier, C. Pierre, Modeling and analysis of mistuned bladed disk vibration: current status and emerging directions, Journal of Propulsion and Power 22 (2) (2006) 384–396. doi:10.2514/1.16345.

[13] J. Colgate, C.-T. Chang, Y.-C. Chiou, W. Liu, L. Keer, Modelling of a hydraulic engine mount focusing on response to sinusoidal and composite excitations, Journal of Sound and Vibration 184 (3) (1995) 503–528. doi:10.1006/jsvi.1995.0330.

[14] M. K. Chamberlain, S. H. Kiefer, J. Banik, Structural analysis methods for the roll-out solar array flight experiment, in: AIAA Scitech 2019 Forum, 2019, p. 2376. doi:10.2514/6.2019-2376.

[15] L. Renson, J.-P. Noël, G. Kerschen, Complex dynamics of a nonlinear aerospace structure: numerical continuation and normal modes, Nonlinear Dynamics 79 (2015) 1293–1309. doi:10.1007/s11071-014-1743-0.

[16] M. Feldman, Non-linear system vibration analysis using hilbert transform–ii. forced vibration analysis method'forcevib', Mechanical Systems and Signal Processing 8 (3) (1994) 309–318. doi:10.1006/mssp.1994.1023.

[17] G. Kerschen, K. Worden, A. F. Vakakis, J.-C. Golinval, Past, present and future of nonlinear system identification in structural dynamics, Mechanical systems and signal processing 20 (3) (2006) 505–592. doi:10.1016/j.ymssp.2005.04.008.

[18] B. Balachandran, A. H. Nayfeh, S. W. Smith, R. S. Pappa, On identification of nonlinear interactions in structures, AIAA Journal 17 (1994) 257–262. doi:10.2514/3.21191.

[19] B. Balachandran, K. A. Khan, Spectral analyses of non-linear interactions, Mechanical Systems and Signal Processing 10 (6) (1996) 711–727. doi:10.1006/mssp.1996.0048.

[20] D. Storer, G. Tomlinson, Recent developments in the measurement and interpretation of higher order transfer functions from non-linear structures, Mechanical Systems and Signal Processing 7 (2) (1993) 173–189. doi:10.1006/mssp.1993.1006.

[21] K. Worden, G. Manson, Random vibrations of a duffing oscillator using the volterra series, Journal of Sound and Vibration 4 (217) (1998) 781–789. doi:10.1016/j.jsv.2004.10.028.

[22] A. Khan, N. Vyas, Application of volterra and wiener theories for nonlinear parameter estimation in a rotor-bearing system, Nonlinear Dynamics 24 (2001) 285–304. doi:10.1023/A:1008352829782.

[23] M. Schetzen, The Volterra and Wiener theories of nonlinear systems, J. Wiley, New York, 1980.

[24] E. Bedrosian, S. O. Rice, The output properties of volterra systems (nonlinear systems with memory) driven by harmonic and gaussian inputs, Proceedings of the IEEE 59 (12) (1971) 1688–1707. doi:10.1109/PROC.1971.8525.

[25] J. Paduart, L. Lauwers, J. Swevers, K. Smolders, J. Schoukens, R. Pintelon, Identification of nonlinear systems using polynomial nonlinear state space models, Automatica 46 (4) (2010) 647–656. doi:10.1016/j.automatica.2010.01.001.

[26] J.-P. Noël, A. F. Esfahani, G. Kerschen, J. Schoukens, A nonlinear state-space approach to hysteresis identification, Mechanical Systems and Signal Processing 84 (2017) 171–184. doi:10.1016/j.ymssp.2016.08.025.

[27] S. B. Cooper, K. Tiels, D. DiMaio, Nonlinear identification of an aero-engine component using polynomial nonlinear state space model, in: Nonlinear Dynamics, Volume 1: Proceedings of the 36th IMAC, A Conference and Exposition on Structural Dynamics 2018, Springer, 2019, pp. 261–273. doi:10.1007/978-3-319-74280-9_27.

[28] J. Decuyper, T. De Troyer, M. Runacres, K. Tiels, J. Schoukens, Nonlinear state-space modelling of the kinematics of an oscillating circular cylinder in a fluid flow, Mechanical Systems and Signal Processing 98 (2018) 209–230. doi:10.1016/j.ymssp.2017.04.048.

[29] M. F. Siddiqui, P. Z. Csurcsia, T. De Troyer, M. C. Runacres, Constructing nonlinear data-driven models from pitching wing experiments using multisine excitation signals, Mechanical Systems and Signal Processing 216 (2024) 111460. doi:10.1016/j.ymssp.2024.111460.

[30] G. Kerschen, M. Peeters, J.-C. Golinval, A. F. Vakakis, Nonlinear normal modes, part i: A useful framework for the structural dynamicist, Mechanical Systems and Signal Processing 23 (1) (2009) 170–194. doi:10.1016/j.ymssp.2008.04.002.

[31] C. Touzé, M. Amabili, O. Thomas, Reduced-order models for large-amplitude vibrations of shells including in-plane inertia, Computer methods in applied mechanics and engineering 197 (21-24) (2008) 2030–2045. doi:10.1016/j.cma.2008.01.002.

[32] D. Anastasio, S. Marchesiello, G. Gatti, P. Gonçalves, A. Shaw, M. Brennan, An investigation into model extrapolation and stability in the system identification of a nonlinear structure, Nonlinear Dynamics 111 (19) (2023) 17653–17665. doi:10.1007/s11071-023-08770-7.

[33] M. Peeters, R. Viguié, G. Sérandour, G. Kerschen, J.-C. Golinval, Nonlinear normal modes, part ii: Toward a practical computation using numerical continuation techniques, Mechanical Systems and Signal Processing 23 (1) (2009) 195–216. doi:10.1016/j.ymssp.2008.04.003.

[34] T. Karaağaçlı, H. N. Özgüven, Experimental modal analysis of nonlinear systems by using response-controlled stepped-sine testing, Mechanical Systems and Signal Processing 146 (2021) 107023. doi:10.1016/j.ymssp.2020.107023.

[35] L. Renson, A. Gonzalez-Buelga, D. A. Barton, S. A. Neild, Robust identification of backbone curves using control-based continuation, Journal of Sound and Vibration 367 (2016) 145–158. doi:10.1016/j.jsv.2015.12.035.

[36] V. Denis, M. Jossic, C. Giraud-Audine, B. Chomette, A. Renault, O. Thomas, Identification of nonlinear modes using phase-locked-loop experimental continuation and normal form, Mechanical Systems and Signal Processing 106 (2018) 430–452. doi:10.1016/j.ymssp.2018.01.014.

[37] M. Song, L. Renson, B. Moaveni, G. Kerschen, Bayesian model updating and class selection of a wing-engine structure with nonlinear connections using nonlinear normal modes, Mechanical Systems and Signal Processing 165 (2022) 108337. doi:10.1016/j.ymssp.2021.108337.

[38] S. F. Masri, T. K. Caughey, A Nonparametric Identification Technique for Nonlinear Dynamic Problems, Journal of Applied Mechanics 46 (2) (1979) 433–447. doi:10.1115/1.3424568.

[39] M. A. Al-Hadid, J. Wright, Developments in the force-state mapping technique for non-linear systems and the extension to the location of non-linear elements in a lumped-parameter system, Mechanical Systems and Signal Processing 3 (3) (1989) 269–290. doi:10.1016/0888-3270(89)90053-8.

[40] S. F. Masri, H. Sassi, T. K. Caughey, Nonparametric Identification of Nearly Arbitrary Nonlinear Systems, Journal of Applied Mechanics 49 (3) (1982) 619–628. doi:10.1115/1.3162537.

[41] C. Martinelli, A. Coraddu, A. Cammarano, Strongly nonlinear multi-degree of freedom systems: Experimental analysis and model identification, Mechanical Systems and Signal Processing 218 (2024) 111532. doi:10.1016/j.ymssp.2024.111532.

[42] A. Sadeqi, S. Moradi, Nonlinear system identification based on restoring force transmissibility of vibrating structures, Mechanical Systems and Signal Processing 172 (2022) 108978. doi:10.1016/j.ymssp.2022.108978.

[43] D. Anastasio, A. Fasana, L. Garibaldi, S. Marchesiello, Nonlinear dynamics of a duffing-like negative stiffness oscillator: Modeling and experimental characterization, Shock and Vibration 2020 (1) (2020) 3593018. doi:10.1155/2020/3593018.

[44] J. Taghipour, H. H. Khodaparast, M. I. Friswell, A. D. Shaw, H. Jalali, N. Jamia, Harmonic-balance-based parameter estimation of nonlinear structures in the presence of multi-harmonic response and force, Mechanical Systems and Signal Processing 162 (2022) 108057. doi:10.1016/j.ymssp.2021.108057.

[45] D. Adams, R. Allemang, A frequency domain method for estimating the parameters of a non-linear structural dynamic model through feedback, Mechanical Systems and Signal Processing 14 (4) (2000) 637–656. doi:10.1006/mssp.2000.1292.

[46] S. Marchesiello, L. Garibaldi, A time domain approach for identifying nonlinear vibrating structures by subspace methods, Mechanical Systems and Signal Processing 22 (1) (2008) 81–101. doi:10.1016/j.ymssp.2007.04.002.

[47] J.-P. Noël, G. Kerschen, Frequency-domain subspace identification for nonlinear mechanical systems, Mechanical Systems and Signal Processing 40 (2) (2013) 701–717. doi:10.1016/j.ymssp.2013.06.034.

[48] J.-P. Noël, S. Marchesiello, G. Kerschen, Subspace-based identification of a nonlinear spacecraft in the time and frequency domains, Mechanical Systems and Signal Processing 43 (1-2) (2014) 217–236. doi:10.1016/j.ymssp.2013.10.016.

[49] D. Anastasio, S. Marchesiello, Nonlinear frequency response curves estimation and stability analysis of randomly excited systems in the subspace framework, Nonlinear Dynamics 111 (9) (2023) 8115–8133. doi:10.1007/s11071-023-08280-6.

[50] X. Liu, G. Cai, A novel time-domain approach for identifying nonlinear structural dynamical system with explicit model based on observer/kalman filter identification method, Journal of Sound and Vibration 578 (2024) 118363. doi:10.1016/j.jsv.2024.118363.

[51] K. Yasuda, S. Kawamura, K. Watanabe, Identification of nonlinear multi-degree-of-freedom systems: presentation of an identification technique, JSME international journal. Ser. 3, Vibration, control engineering, engineering for industry 31 (1) (1988) 8–14. doi:10.1299/jsmec1988.31.8.

[52] K. Yasuda, K. Kamiya, M. Komakine, Experimental identification technique of vibrating structures with geometrical nonlinearity, Journal of Applied Mechanics 64 (2) (1997) 275–280. doi:10.1115/1.2787304.

[53] K. Yasuda, K. Kimiya, Identification of a nonlinear beam: Proposition of an identitication technique, JSME international journal. Ser. 3, Vibration, control engineering, engineering for industry 33 (4) (1990) 535–540. doi:10.1299/jsmec1988.33.535.

[54] B. Feeny, C.-M. Yuan, J. Cusumano, Parametric identification of an experimental magneto-elastic oscillator, Journal of Sound and Vibration 247 (5) (2001) 785–806. doi:10.1006/jsvi.2001.3694.

[55] M. Thothadri, R. Casas, F. Moon, R. D'andrea, C. Johnson, Nonlinear system identification of multi-degree-of-freedom systems, Nonlinear Dynamics 32 (2003) 307–322. doi:10.1023/A:1024489210804.

[56] M. Amabili, F. Alijani, J. Delannoy, Damping for large-amplitude vibrations of plates and curved panels, part 2: Identification and comparisons, International Journal of Non-Linear Mechanics 85 (2016) 226–240. doi:10.1016/j.ijnonlinmec.2016.05.004.

[57] M. Thothadri, F. Moon, Nonlinear system identification of systems with periodic limit-cycle response, Nonlinear Dynamics 39 (2005) 63–77. doi:10.1007/s11071-005-1914-0.

[58] M. W. Ahmadi, T. L. Hill, J. Z. Jiang, S. A. Neild, Reduced-order model-inspired system identification of geometrically nonlinear structures: application to a nonlinear cantilever-type structure, Nonlinear Dynamics 111 (19) (2023) 17887–17907. doi:10.1007/s11071-023-08813-z.

[59] S. L. Brunton, J. L. Proctor, J. N. Kutz, Discovering governing equations from data by sparse identification of nonlinear dynamical systems, Proceedings of the National Academy of Sciences 113 (15) (2016) 3932–3937. doi:10.1073/pnas.1517384113.

[60] U. Fasel, J. N. Kutz, B. W. Brunton, S. L. Brunton, Ensemble-sindy: Robust sparse model discovery in the low-data, high-noise limit, with active learning and control, Proceedings of the Royal Society A 478 (2260) (2022) 20210904. doi:10.1098/rspa.2021.0904.

[61] Q. Liu, J. Cao, Y. Zhang, Z. Zhao, G. Kerschen, X. Jing, Interpretable sparse identification of a bistable nonlinear energy sink, Mechanical Systems and Signal Processing 193 (2023) 110254. doi:10.1016/j.ymssp.2023.110254.

[62] M. Lin, C. Cheng, Z. Peng, X. Dong, Y. Qu, G. Meng, Nonlinear dynamical system identification using the sparse regression and separable least squares methods, Journal of Sound and Vibration 505 (2021) 116141. doi:10.1016/j.jsv.2021.116141.

[63] S. Safari, J. M. L. Monsalve, Direct optimisation based model selection and parameter estimation using time-domain data for identifying localised nonlinearities, Journal of Sound and Vibration 501 (2021) 116056. doi:10.1016/j.jsv.2021.116056.

[64] R. Nayek, R. Fuentes, K. Worden, E. J. Cross, On spike-and-slab priors for bayesian equation discovery of nonlinear dynamical systems via sparse linear regression, Mechanical Systems and Signal Processing 161 (2021) 107986. doi:10.1016/j.ymssp.2021.107986.

[65] Z. Lai, S. Nagarajaiah, Sparse structural system identification method for nonlinear dynamic systems with hysteresis/inelastic behavior, Mechanical Systems and Signal Processing 117 (2019) 813–842. doi:10.1016/j.ymssp.2018.08.033.

[66] A. Pal, S. Nagarajaiah, Sparsity promoting algorithm for identification of nonlinear dynamic system based on unscented kalman filter using novel selective thresholding and penalty-based model selection, Mechanical Systems and Signal Processing 212 (2024) 111301. doi:10.1016/j.ymssp.2024.111301.

[67] G. T. Naozuka, H. L. Rocha, R. S. Silva, R. C. Almeida, Sindy-sa framework: enhancing nonlinear system identification with sensitivity analysis, Nonlinear Dynamics 110 (3) (2022) 2589–2609. doi:10.1007/s11071-022-07755-2.

[68] C. Lathourakis, A. Cicirello, Physics enhanced sparse identification of dynamical systems with discontinuous nonlinearities, Nonlinear Dynamics 112 (13) (2024) 11237–11264. doi:10.1007/s11071-024-09652-2.

[69] B. Peeters, H. Van der Auweraer, P. Guillaume, J. Leuridan, The polymax frequency-domain method: a new standard for modal parameter estimation?, Shock and Vibration 11 (3-4) (2004) 395–409. doi:10.1155/2004/523692.

[70] S. Lang, Real and functional analysis, Vol. 142, Springer Science & Business Media, 2012. doi:10.1007/978-1-4612-0897-6.

[71] G. Tomlinson, Force distortion in resonance testing of structures with electro-dynamic vibration exciters, Journal of Sound and Vibration 63 (3) (1979) 337–350. doi:10.1016/0022-460X(79)90678-3.

[72] M. Krack, J. Gross, Harmonic balance for nonlinear vibration problems, Vol. 1, Springer, 2019. doi:10.1007/978-3-030-14023-6.

[73] T. Breunung, B. Balachandran, Noise color influence on escape times in nonlinear oscillators - experimental and numerical results, Theoretical and Applied Mechanics Letters 13 (2) (2023) 100420. doi:10.1016/j.taml.2022.100420.

[74] J. N. Kutz, S. L. Brunton, Parsimony as the ultimate regularizer for physics-informed machine learning, Nonlinear Dynamics 107 (3) (2022) 1801–1817. doi:10.1007/s11071-021-07118-3.

[75] R. Tibshirani, Regression shrinkage and selection via the lasso, Journal of the Royal Statistical Society: Series B (Methodological) 58 (1) (1996) 267–288. doi:10.1016/j.cma.2008.01.002.

[76] T. Hastie, R. Tibshirani, J. H. Friedman, J. H. Friedman, The elements of statistical learning: data mining, inference, and prediction, Vol. 2, Springer, 2009. doi:10.1007/978-0-387-84858-7.

[77] T. Hastie, R. Tibshirani, M. Wainwright, Statistical learning with sparsity: the lasso and generalizations, CRC press, 2015. doi:10.1201/b18401.

[78] Brbtesting, https://github.com/mattiacenedese/BRBtesting, accessed: 2022-04-08.

[79] E. J. Doedel, A. R. Champneys, F. Dercole, T. F. Fairgrieve, Y. A. Kuznetsov, B. Oldeman, R. Paffenroth, B. Sandstede, X. Wang, C. Zhang, Auto-07p: Continuation and bifurcation software for ordinary differential equations (2007).

[80] H. Dankowicz, F. Schilder, Recipes for Continuation, SIAM, 2013. doi:10.1137/1.9781611972573.

[81] A. Dhooge, W. Govaerts, Y. A. Kuznetsov, Matcont: a matlab package for numerical bifurcation analysis of odes, ACM Transactions on Mathematical Software (TOMS) 29 (2) (2003) 141–164. doi:10.1145/779359.779362.

[82] M. F. Daqaq, R. Masana, A. Erturk, D. Dane Quinn, On the role of nonlinearities in vibratory energy harvesting: a critical review and discussion, Applied Mechanics Reviews 66 (4) (2014). doi:10.1115/1.4026278.

[83] F. Moon, P. J. Holmes, A magnetoelastic strange attractor, Journal of Sound and Vibration 65 (2) (1979) 275–296. doi:10.1016/0022-460X(79)90520-0.

[84] M. Schüssler, O. Nelles, Extrapolation behavior comparison of nonlinear state space models, IFAC-PapersOnLine 54 (7) (2021) 487–492. doi:10.1016/j.ifacol.2021.08.407.

[85] T. Breunung, G. Haller, Explicit backbone curves from spectral submanifolds of forced-damped nonlinear mechanical systems, Proceedings of the Royal Society A: Mathematical, Physical and Engineering Sciences 474 (2213) (2018) 20180083. doi:10.1098/rspa.2018.0083.

[86] A. Sievers, S. Takeno, Intrinsic localized modes in anharmonic crystals, Physical Review Letters 61 (8) (1988) 970. doi:10.1137/1.9781611972573.

[87] A. F. Vakais, C. Cetinkaya, Mode localization in a class of multidegree-of-freedom nonlinear systems with cyclic symmetry, SIAM Journal on Applied Mathematics 53 (1) (1993) 265–282. doi:10.1137/0153016.

[88] A. Dick, B. Balachandran, C. Mote, Intrinsic localized modes in microresonator arrays and their relationship to nonlinear vibration modes, Nonlinear Dynamics 54 (2008) 13–29. doi:10.1007/s11071-007-9288-0.

[89] B. Balachandran, T. Breunung, G. D. Acar, A. Alofi, J. A. Yorke, Dynamics of circular oscillator arrays subjected to noise, Nonlinear Dynamics 108 (1) (2022) 1–14. doi:10.1007/s11071-021-07165-w.

[90] M. Jin, G. Kosova, M. Cenedese, W. Chen, A. Singh, D. Jana, M. R. Brake, C. W. Schwingshackl, S. Nagarajaiah, K. J. Moore, et al., Measurement and identification of the nonlinear dynamics of a jointed structure using full-field data; part ii-nonlinear system identification, Mechanical Systems and Signal Processing 166 (2022) 108402. doi:10.1016/j.ymssp.2021.108402.

[91] H. Cho, B. Jeong, M.-F. Yu, A. F. Vakakis, D. M. McFarland, L. A. Bergman, Nonlinear hardening and softening resonances in micromechanical cantilever-nanotube systems originated from nanoscale geometric nonlinearities, International Journal of Solids and Structures 49 (15-16) (2012) 2059–2065. doi:10.1016/j.ijsolstr.2012.04.016.

[92] X. Ma, L. Bergman, A. Vakakis, Identification of bolted joints through laser vibrometry, Journal of Sound and Vibration 246 (3) (2001) 441–460. doi:10.1006/jsvi.2001.3573.

[93] D. J. Segalman, A Four-Parameter Iwan Model for Lap-Type Joints, Journal of Applied Mechanics 72 (5) (2005) 752–760. doi:10.1115/1.1989354.

[94] L. Gaul, R. Nitsche, The Role of Friction in Mechanical Joints, Applied Mechanics Reviews 54 (2) (2001) 93–106. doi:10.1115/1.3097294.

[95] L. Gaul, J. Lenz, Nonlinear dynamics of structures assembled by bolted joints, Acta Mechanica 125 (1-4) (1997) 169–181. doi:10.1007/BF01177306.

[96] R. Ibrahim, C. Pettit, Uncertainties and dynamic problems of bolted joints and other fasteners, Journal of Sound and Vibration 279 (3-5) (2005) 857–936. doi:10.1016/j.jsv.2003.11.064.

[97] M. Brake, C. Schwingshackl, P. Reuß, Observations of variability and repeatability in jointed structures, Mechanical Systems and Signal Processing 129 (2019) 282–307. doi:10.1016/j.ymssp.2019.04.020.

[98] W. Chen, D. Jana, A. Singh, M. Jin, M. Cenedese, G. Kosova, M. R. Brake, C. W. Schwingshackl, S. Nagarajaiah, K. J. Moore, et al., Measurement and identification of the nonlinear dynamics of a jointed structure using full-field data, part i: Measurement of nonlinear dynamics, Mechanical Systems and Signal Processing 166 (2022) 108401. doi:10.1016/j.ymssp.2021.108401.

[99] M. Cenedese, J. Axås, B. Bäuerlein, K. Avila, G. Haller, Data-driven modeling and prediction of non-linearizable dynamics via spectral submanifolds, Nature Communications 13 (1) (2022) 872. doi:10.1038/s41467-022-28518-y.

[100] M. Cenedese, J. Axås, H. Yang, M. Eriten, G. Haller, Data-driven nonlinear model reduction to spectral submanifolds in mechanical systems, Philosophical Transactions of the Royal Society A 380 (2229) (2022) 20210194. doi:10.1098/rsta.2021.0194.

[101] T. Breunung, L. Cilenti, J. M. You, B. Balachandran, Robust identification of nonlinear oscillators from frequency response data, in: Society for Experimental Mechanics Annual Conference and Exposition, Springer, 2023, pp. 11–13. doi:10.1007/978-3-031-36999-5_2.

[102] M. Peeters, G. Kerschen, J.-C. Golinval, Dynamic testing of nonlinear vibrating structures using nonlinear normal modes, Journal of Sound and Vibration 330 (3) (2011) 486–509. doi:10.1016/j.jsv.2010.08.028.